Tundra
oil and gas ltd.

January 26, 1994

Manitoba Energy and Mines
Petroleum Branch
555 - 330 Graham Avenue
Winnipeg, Manitoba
R3C 4E3

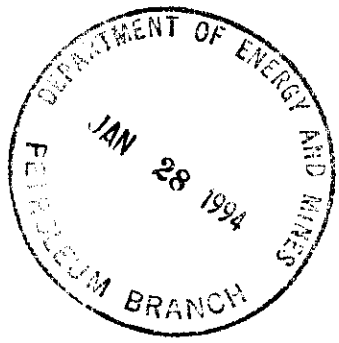

Attention: Mr. J. Fox, P.Eng.
Chief Petroleum Engineer

Dear John,

RE: Goodlands Relative Permeability Study
Well 4-14-1-24 W1M

Please find attached the referenced special core study for your files that Tundra recently completed.

Should you have any questions, I can be reached at 934-5853.

Yours truly,

TUNDRA OIL AND GAS LTD.

George Czyzewski, P.Eng.
Senior Reservoir Engineer

1111 - One Lombard Place, Winnipeg, Manitoba R3B 0X4 Telephone: (204) 934-5850 Fax: (204) 934-5820

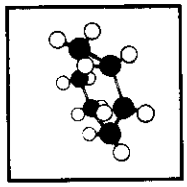

Hycal
ENERGY RESEARCH LABORATORIES LTD.

TUNDRA - GOODLANDS
RELATIVE PERMEABILITY STUDY

Prepared For

Tundra Oil & Gas Ltd.

Prepared By

Hycal Energy Research Laboratories Ltd.

January 25, 1994

93-125

1338A - 36th Avenue N.E., Calgary, Alberta, Canada T2E 6T6
Telephone (403) 250-5800 Telex 03-821172 CGY Fax: (403) 291-0481

TABLE OF CONTENTS

TABLE OF CONTENTS

LIST OF TABLES

LIST OF FIGURES

LIST APPENDICES

SUMMARY

SUMMARY

At the request of Tundra Oil & Gas Ltd., Hycal Energy Research Laboratories Ltd. conducted laboratory tests to determine a water-dead oil relative permeability profile using restored core material from the 908.64 to 914.46 m interval of well 4-14-1-24 W1M in the Spearfish formation of the Goodlands field. Major results of the study are summarized as follows:

Water-Dead Oil Relative Permeability Tests

Water-dead oil relative permeability tests were conducted to generate the water-oil relative permeability profile as well as endpoint saturation and permeability data. These endpoint data are summarized as follows:

Core Stack #1					
	So	**Sw**	**k_o (mD)**	**k_w (mD)**	**Relative Permeability**
Initial Oilflood (@ Sw_i)	0.579	0.421	1.17	--	0.308
Endpoint Waterflood (@ So_r)	0.235	0.765	--	0.38	0.100
k_{abs} = 3.80 mD					
Porosity = 19.3%					
Recovery (PV) = 34.4%					
Recovery (HCPV) = 59.4%					

A second core stack composed of core samples representing the lower permeability range of the reservoir was also tested but had insufficient liquid permeability to be waterflooded.

INTRODUCTION

INTRODUCTION

At the request of George Czyzewski of Tundra Oil & Gas Ltd., Hycal conducted an experiment to determine a water-dead oil relative permeability profile using reservoir core material from the Spearfish formation in the Goodlands area. This report describes the experimental equipment and procedures used and presents the results of the test program.

DESCRIPTION OF EQUIPMENT

DESCRIPTION OF EQUIPMENT

General Displacement Test Equipment

Equipment that is used in conventional core/fluid displacement experiments is common to most coreflow evaluation techniques. Detailed schematics of the specific apparatus configuration are provided in the Figures section of this report. General descriptions of the basic components of these tests appear in the following paragraphs.

Core Mounting

The core sample is placed in a 3.81 cm ID, 0.692 cm WT heavy lead sleeve. The ductility of the lead sleeve allows a confining overburden pressure to be transferred to the core to simulate reservoir pressure. The core, mounted within the lead sleeve, is placed inside a 7.5 cm ID steel core holder that can simulate reservoir pressures of up to 68.9 mPa. This pressure is applied by filling the annular space between the lead sleeve and the core holder with formation water. The water is then compressed with a hydraulic pump to obtain the desired overburden pressure.

The core holder ends each contain two ports to facilitate fluid displacement and pressure measurements at each end of the core. The portions of the core holder directly adjacent to the injection and production ends of the core are equipped with radial distribution plates to ensure evenly distributed fluid flow into and out of the core specimen.

Pressure Measurement

Pressure differential is monitored using a Validyne pressure transducer. The transducer is mounted directly across the core and measures the pressure differential between the injection and production ends. The pressure transducer has a range of 0 to 350 or 0 to 3500 kPa and is accurate to 0.01% of the full scale value. The signal from the pressure transducer can be

connected to a strip chart recorder that provides a continuous pressure profile of the test. A digital readout also appears on a multi-channel Validyne terminal from which the test operator records pressure readings during the displacement processes.

Fluid Displacement

A Ruska displacement pump is used to inject fluids into the core. The pump can inject fluids at rates from 1 to 8200 cm^3/hr and at pressures of up to 68.9 MPa, with an accuracy of ± 0.01 cm^3. The pump is filled with distilled water that displaces live crude oil or varsol (that then displaces test brine) into the core. The experimental system has been designed to minimize dead volumes and to ensure that the entire system is at pressure equilibrium prior to any fluid change. Backpressure on the system (for full reservoir condition tests) is controlled using a 316 SS controlling backpressure regulator accurate to 0.5% of the setpoint value. This regulator allows for the smooth production of fluids from the system at any required flowrate and setpoint pressure.

All injection fluids are filtered to 0.5 microns before use to remove any potentially plugging suspended particles (unless unfiltered fluids are requested). An in-line 0.5 micron filter is also present directly before the core as a backup filtration system (removable if unfiltered fluids are wanted).

EXPERIMENTAL PROCEDURE

EXPERIMENTAL PROCEDURE

Core Samples

Previously extracted full diameter core samples were obtained from Tundra Oil & Gas from which twelve 3.81 cm OD small plugs could be removed to be used as the core material for laboratory testing. All small core plugs were drilled using 5% KCl as a lubricating fluid to avoid damage to in-situ clays and prevent any other damage to the core during drilling. Routine permeability and porosity measurements were conducted on the small plug samples to aid in the selection of core material for testing.

Test Fluids

Adequate volumes of produced water and stock tank oil were received from Tundra Oil & Gas Ltd. for use in these laboratory tests. No additional fluid preparation was required.

Wettability Restoration

All the core samples used in this study had been previously extracted and cleaned. An intensive restoration procedure was used to attempt to restore the core wettability to in-situ conditions. The cores to be restored were mounted in lead sleeves, evacuated and then saturated with formation brine. This brine was circulated in the core for one week to establish an initial water saturation that would rehydrate the in-situ clays. This was followed by the circulation of unoxidized dead crude oil at reservoir temperature for a recommended period of six weeks. At the beginning of each week a fresh supply of oil was circulated through the core for one day and then left to react with the core for six days. The process was repeated for six weeks. This procedure is very important if the rock has a natural tendency to become oil-wet because under these circumstances it will allow the core material to become oil-wet due to the adsorption of the oil heavy ends onto the pore walls.

Water-Dead Oil Relative Permeability Tests - Composite Stack

The following procedure was used for the water-dead oil relative permeability test at reservoir temperature:

1. Mount the composite stack and place in the oven at reservoir temperature with the specified net overburden pressure.

2. Inject the dead oil into the core to determine the initial baseline permeability to oil.

3. Begin waterflooding the core with formation brine at a low rate and continue until no additional oil is being produced. During this displacement measure the pressure drop across the core and the water and oil production rates to calculate the saturation and relative permeability values.

4. Run several endpoint waterflood tests at higher rates to ensure that the relative permeability data at the endpoint are representative.

5. At the conclusion of the test, depressurize the core to atmospheric pressure and subject to Dean-Stark extraction to calculate the material balance closure and measure exact fluid saturations.

RESULTS AND DISCUSSION

RESULTS AND DISCUSSION

Core Selection and Restoration

The results of the permeability and porosity measurements conducted on the small plugs drilled are presented in Table 1. Based on this information, plugs #26A, #26B and #26C (stack #1) and plugs #10, #29A and #29B (stack #2) were selected for restoration. Restoration was conducted for the full six week period as described in the experimental procedure.

Core Stack #1 - Oil-Water Relative Permeability Test

Composite core stack #1, composed of core plugs #26A, #26B and #26C, had a length of 21.94 cm and a cross sectional area of 10.93 cm^2. Post-test composite average porosity on the stack was determined to be 19.3%. The core plugs were mounted as described in the Experimental Procedure section of the report. Table 2 provides a summary of core and fluid parameters for the waterflood test conducted on this core stack.

Table 3 provides a summary of the oil and water saturations in the core after each displacement step phase and the measured endpoint permeability and relative permeability for each step. Initial oil and water saturations in the restored state plug had values of 0.579 and 0.421 respectively.

Initial permeability to the displacing oil phase had a value of 1.17 mD. Absolute fluid permeability for the core stack was estimated to be 3.8 mD from the extrapolation of the k_{ro} curve to a 1.00 value at 100% oil saturation. Subsequent water and oil phase relative permeabilities were calculated using this estimated absolute permeability.

Reported fluid permeabilities are likely less than routine core analysis air permeabilities for this core material. This can be attributed to the following factors:

1. Relative permeability effects associated with the presence of an irreducible water phase saturation in the core.

2. Standard air permeability measurements are non-Klinkenberg slip corrected. Correction for surface slippage effects often results in a substantial reduction in effective absolute permeability, particularly for lower permeability core material.

3. The application of reservoir pore pressure instead of a nominal overburden pressure (1378 kPa) at which the routine gas permeabilities are measured can substantially reduce permeability due to physical compressure of the flow channels. Increases in temperature have also been noted to have a reducing effect on permeability.

4. Extracted and dried core material in general seems to exhibit higher air permeabilities (even if overburden pressure and temperature are held constant) than fluid saturated cores. This phenomenon is believed to be related to desiccation of the clays and other hydratable materials in the matrix caused by the extraction and drying process. Introduction of water into the matrix appears to rehydrate these materials causing a change in internal matrix flow geometry and a reduction in apparent permeability.

Table 4 contains the experimental differential pressure and oil production history from the waterflood. The oil production data and differential pressure data have been plotted as a function of time and appear as Figures 2 and 3 respectively.

The waterflood resulted in final oil and water saturation values of 0.235 and 0.765 after 2.29 pore volumes of water injection. This represents a recovery of 59.4% of the initial oil-in-place in the core prior to waterflooding. Endpoint permeability to water at this saturation level had a value of 0.38 mD yielding a water endpoint relative permeability value of 0.100. The waterflood was conducted at an injection rate of 6 cc/hr which corresponds to an absolute interstitial velocity of 2.84 cm/hr (assuming that all the porosity is available for flow).

The relative permeability data presented in this report was generated by a computer simulation as described in a paper by Bennion et al. A copy of this paper is also included in the appendix of this report. The program required information concerning rock and fluid properties, as well as the differential pressure and production history over the course of the test. The

program initially assumed values for the pressure differential and recovery data, and then compared these values to the experimental data and computed the least square error. The program continued to iterate in this fashion until the minimum least square error was obtained. The two-phase flow equation was solved using finite difference techniques, and the model included capillary pressure effects.

Table 5 provides a summary of the oil-water relative permeability data as generated by the simulator for the waterflood conducted on the stack. The relative permeability data have been plotted vs water saturation on both cartesian and semi-log co-ordinates and appear as Figures 4 and 5 respectively.

At the conclusion of the test, the core was disassembled and subjected to Dean-Stark analysis to determine residual oil, gas and water saturations. These saturations, together with produced fluid volumes which were recorded throughout the test series, were used as a basis for the calculation of all of the previously discussed saturation data.

Core Stack #2 - Oil-Water Relative Permeability Test

Composite core stack #2, composed of cores #10, #29A and #29B, was mounted for testing as described in the Experimental Procedure section of this report. Attempts to establish a baseline permeability to crude oil were unsuccessful due to the extremely low liquid permeability of the composite core stack. The core stack was then dismantled and individual attempts were made to establish a baseline permeability on single plugs #10 and #29B. Neither attempt established a stabilized baseline permeability to crude oil at a reasonable injection pressure. The testing of these core samples was subsequently terminated.

Data Diskette Summary

A 3½" high density data diskette is included at the end of the report. This diskette contains all pertinent numerical information from the test series summarized in Lotus 1-2-3 style spreadsheet format. This will facilitate the plotting and manipulation of the data as required. A summary of the worksheet files contained on the data diskette is as follows:

File Name	Contents
TABLE4.WK1	Core #1 - Water-Oil Relative Permeability Differential Pressure and Production
TABLE5.WK1	Core #1 - Water-Oil Relative Permeability Relative Permeability Data

CONCLUSIONS

CONCLUSIONS

At the request of Tundra Oil and Gas Ltd, Hycal conducted a water-dead oil relative permeability test on core samples from the Goodlands area well 4-14-1-24 W1M for the purpose of determining waterflood feasibility.

Relative permeability tests on the core material were conducted using produced water and dead crude oil. Tundra personnel were informed, before this study was initiated, as to the limitations of dead crude oil in providing representative mobility ratio and interfacial tension parameters during the waterflood. Tundra personnel decided that the use of dead crude oil would adequately represent reservoir conditions since gas production from this well was generally insignificant. The conclusions of this study are as follows:

1. The laboratory waterflood conducted on stack #1 indicated an ultimate recovery of 59.4% of the original oil-in-place (OOIP) after 2.29 pore volumes of water injection. This represents 34.4% of the matrix pore volume. In evaluating the recovery values, it is important to note that the laboratory experiments are microscale representations of the field scenario and that macroscale phenomena such as gravity segregation, permeability channels, natural barriers, etc. may override the displacement efficiency exhibited in the experiments. Recovery values from the experiments are most representative of similar quality reservoir material in the swept zone.

2. The history match simulation conducted to evaluate the relative permeability curve profiles was characterized by a very low least mean error for the final curve fit. Experimental production and pressure history profiles were smooth and no manipulation of the data was required to obtain the relative permeability profiles during the simulation phase of the data evaluation.

3. The unsuccessful attempts to waterflood the lower quality core samples suggests that recovery from the low permeability regions of the reservoir would be expected to be very low due to the high pressure gradient required to mobilize the fluid. In the presence of higher permeability flow channels in the reservoir, these low quality regions would most likely remain unswept by the waterfront as it preferentially fingers through more permeable regions.

TABLES

TABLE 1
TUNDRA - GOODLANDS
RELATIVE PERMEABILITY STUDY
ROUTINE CORE ANALYSIS

Core No.	Depth (m)	Permeability (md)	Porosity (Fraction)	Grain Density
8A	908.64	3.70	18.0	2744
8B	908.64	1.19	18.2	2703
10	909.05	0.98	15.9	2734
18	910.60	1.50	10.1	2802
21	911.34	0.45	15.1	2703
26A	912.60	3.86	21.0	2696
26B	912.60	5.61	20.2	2698
26C	912.60	8.58	17.8	2721
29A	913.40	0.42	17.4	2717
29B	913.40	0.76	16.8	2720
34A	914.46	0.19	8.8	2780
34B	914.46	1.90	17.9	2707

TABLE 2
TUNDRA - GOODLANDS
RELATIVE PERMEABILITY STUDY
CORE STACK #1 - WATER-OIL RELATIVE PERMEABILITY
CORE AND TEST PARAMETERS

Core Stack Number	1
Core Stack Configuration (from inlet)	26A, 26B, 26C
Depth (m)	912.60
Field Name	Goodlands
Well Location	4-14-1-24 W1M
Stack Length (cm)	21.94
Diameter (cm)	3.73
Effective Flow Area (cm^2)	10.93
Bulk Volume (cm^3)	239.74
Porosity (fraction)	0.193
Pore Volume (cm^3)	46.21
Initial Water Saturation (fraction)	0.421
Final Water Saturation (fraction)	0.765
Water Viscosity @ 28°C (mPa•s)	1.26
Oil Viscosity @ 28°C (mPa•s)	6.86
Test Temperature (°C)	28
Displacement Rate (cc/hr)	6.0
Backpressure (kPag)	0
Net Overburden Pressure (kPag)	8500

TABLE 3
TUNDRA - GOODLANDS
RELATIVE PERMEABILITY STUDY
CORE STACK #1 - WATER-OIL RELATIVE PERMEABILITY
SATURATION AND PERMEABILITY SUMMARY

Test Phase	So	Sw	Permeability		Relative Permeability
			$(\mu m)^2 \times 10^{-3}$	mD	
Absolute Liquid Permeability	1.000	0.000	3.75	3.80	1.000
Initial Oil Permeability (@ Sw_i)	0.579	0.421	1.15	1.17	0.308
Final Water Permeability (@ So_r)	0.235	0.765	0.37	0.38	0.100

* Absolute permeability is determined by extrapolating the k_{ro} curve to 1.0 at Sw = 0.0

TABLE 4
TUNDRA - GOODLANDS
RELATIVE PERMEABILITY STUDY
CORE STACK #1 - WATER-OIL RELATIVE PERMEABILITY
DIFFERENTIAL PRESSURE & PRODUCTION

Cuml Injection (PV)	Cuml Production (PV)	Pressure (MPa)
0.079	0.079	2.29259
0.111	0.111	2.41325
0.144	0.144	2.44773
0.157	0.157	2.39066
0.195	0.170	2.19211
0.216	0.178	2.07405
0.433	0.259	1.58651
0.649	0.294	1.44359
0.866	0.316	1.32401
1.298	0.329	1.22670
1.731	0.334	1.17366
2.288	0.342	1.10545

TABLE 5
TUNDRA - GOODLANDS
RELATIVE PERMEABILITY STUDY
CORE STACK #1 - WATER-OIL RELATIVE PERMEABILITY
RELATIVE PERMEABILITY DATA

Water Saturation	Relative Permeability	
	k_{rw}	k_{ro}
0.423	0.00000	0.30790
0.440	0.00005	0.28230
0.457	0.00014	0.25750
0.474	0.00030	0.23380
0.491	0.00060	0.21090
0.509	0.00111	0.18910
0.526	0.00190	0.16820
0.543	0.00308	0.14840
0.560	0.00472	0.12960
0.577	0.00693	0.11180
0.594	0.00981	0.09520
0.611	0.01349	0.07966
0.628	0.01806	0.06529
0.645	0.02366	0.05211
0.662	0.03040	0.04017
0.679	0.03843	0.02954
0.697	0.04787	0.02030
0.714	0.05886	0.01252
0.731	0.07155	0.00635
0.748	0.08608	0.00201
0.765	0.10260	0.00000

FIGURES

FIGURE 1
TUNDRA - GOODLANDS
RELATIVE PERMEABILITY STUDY
RESERVOIR CONDITION FLUID LEAKOFF APPARATUS

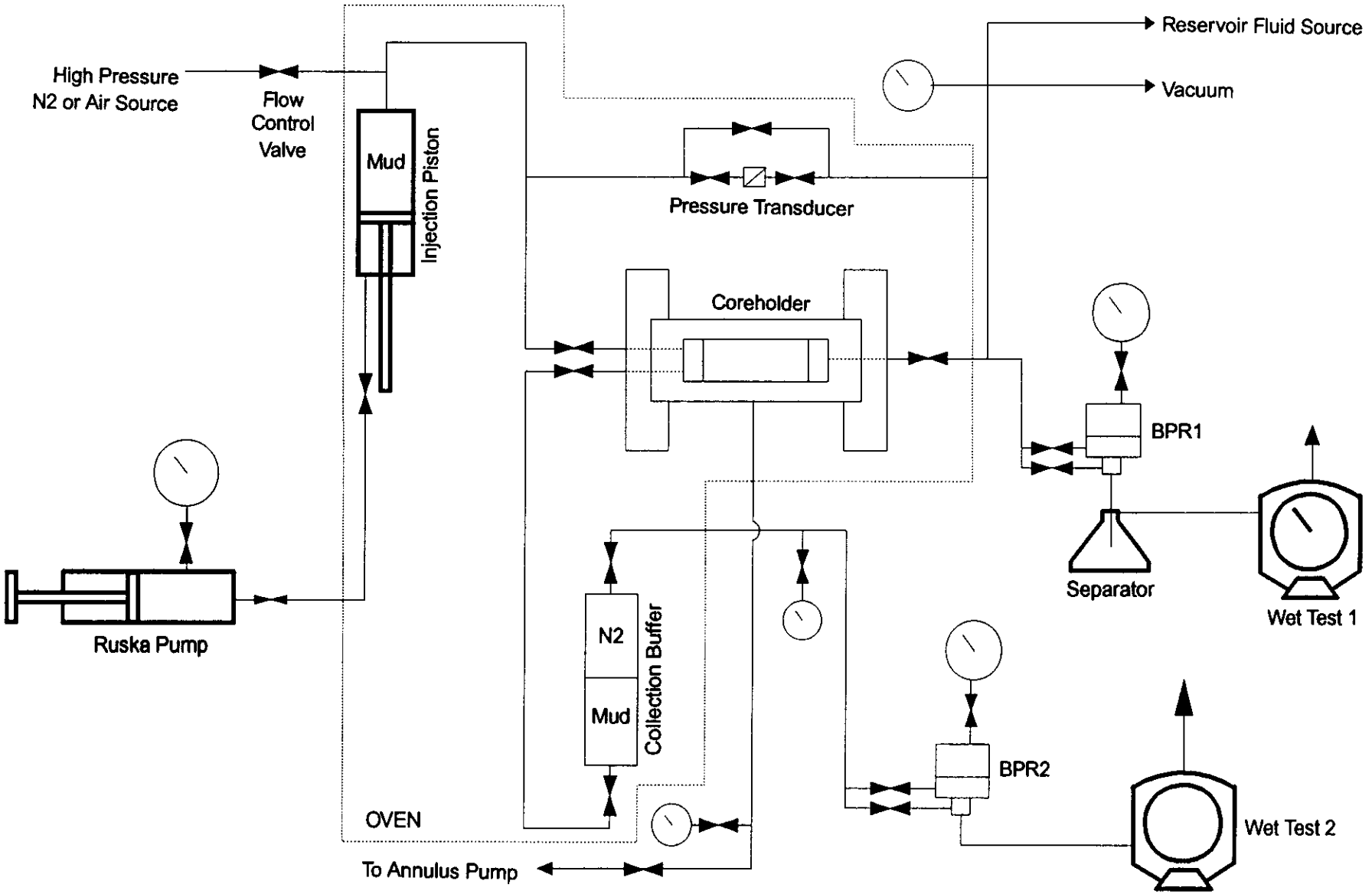

Hycal

FIGURE 2
TUNDRA - GOODLANDS
RELATIVE PERMEABILITY STUDY
CORE STACK #1 - WATER-OIL RELATIVE PERMEABILITY
CUML PRODUCTION vs CUML INJECTION

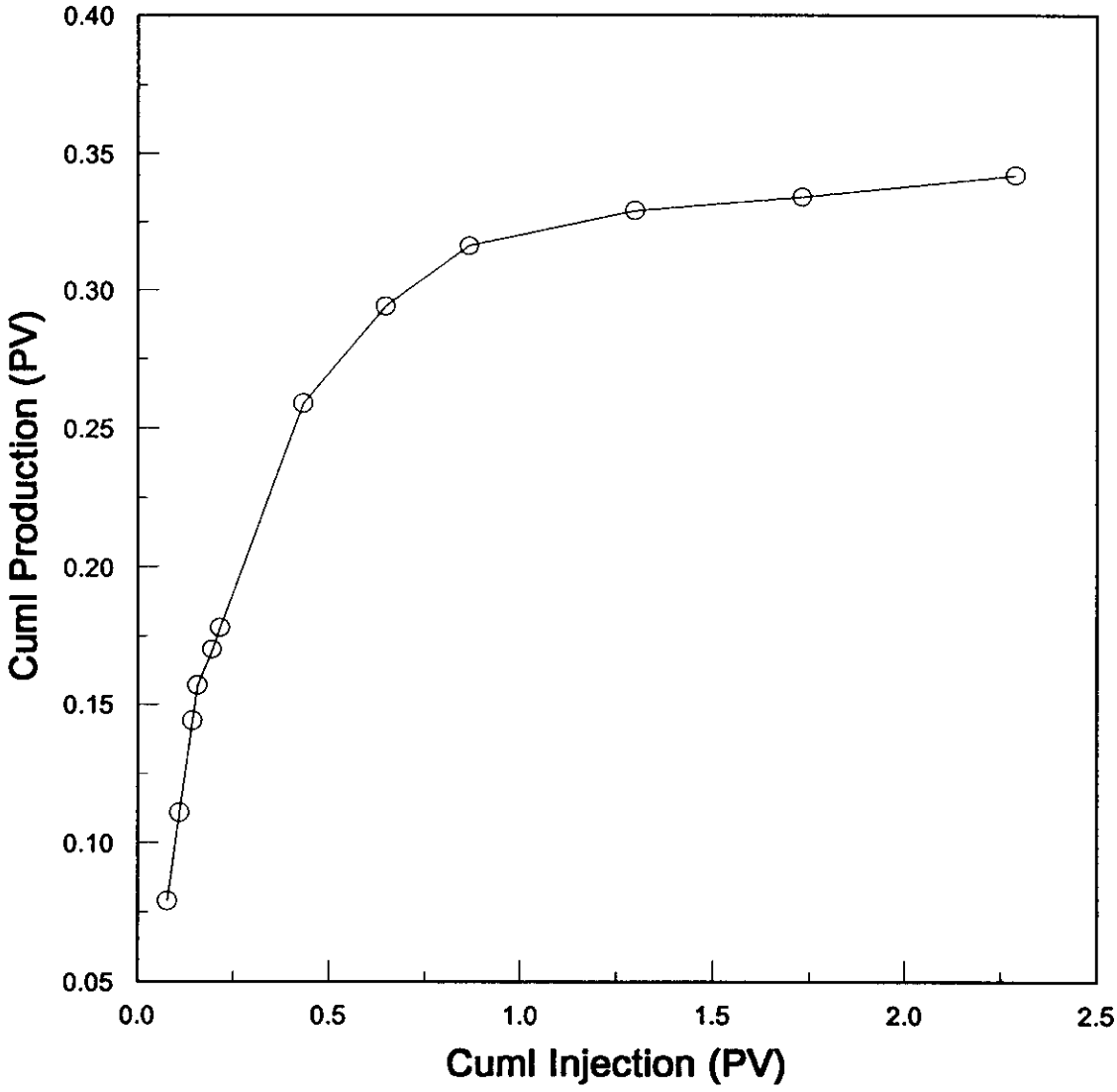

FIGURE 3
TUNDRA - GOODLANDS
RELATIVE PERMEABILITY STUDY
CORE STACK #1 - WATER-OIL RELATIVE PERMEABILITY
PRESSURE vs CUML INJECTION

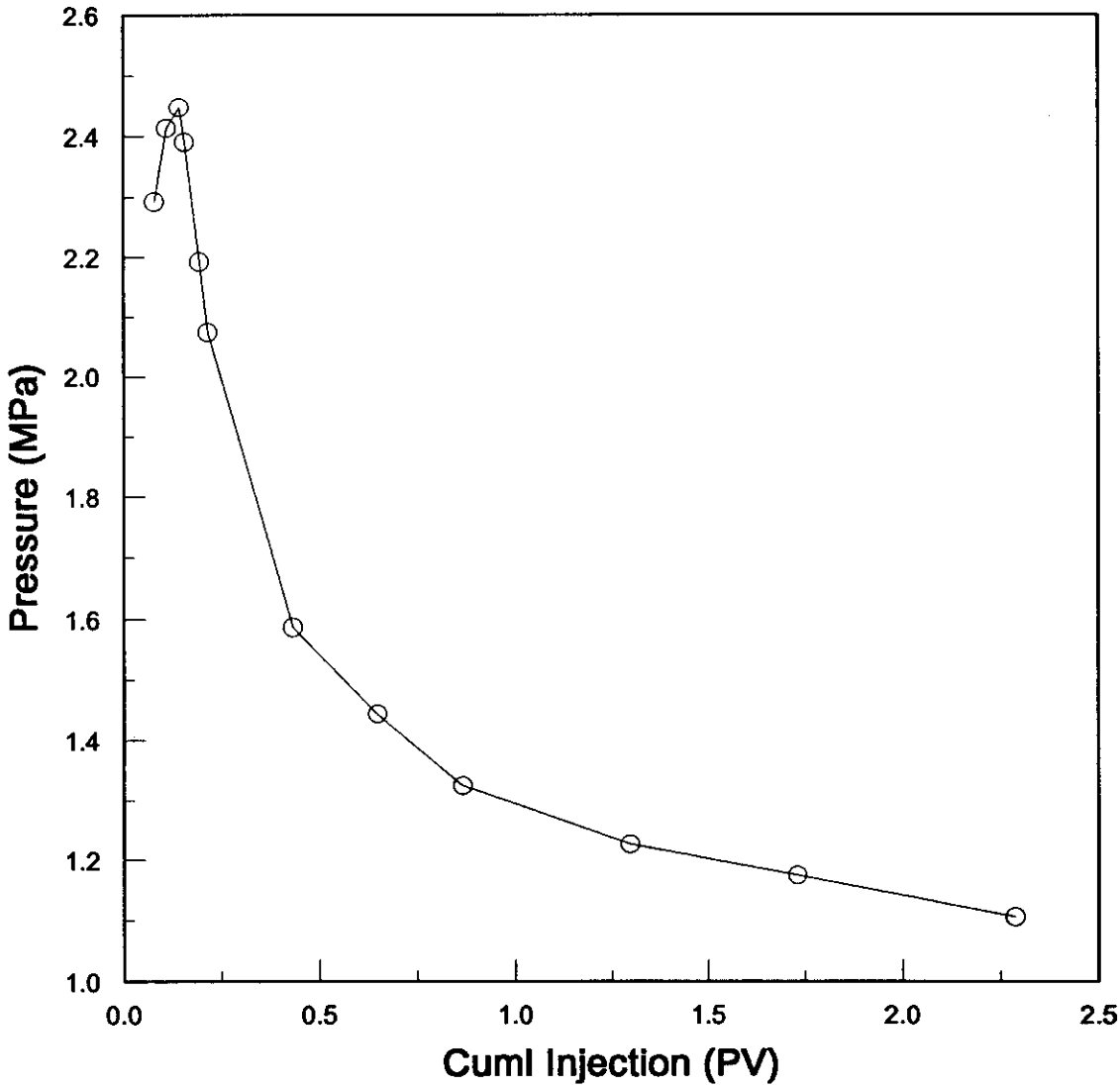

FIGURE 4
TUNDRA - GOODLANDS
RELATIVE PERMEABILITY STUDY
CORE STACK #1 - WATER-OIL RELATIVE PERMEABILITY
RELATIVE PERMEABILITY vs WATER SATURATION

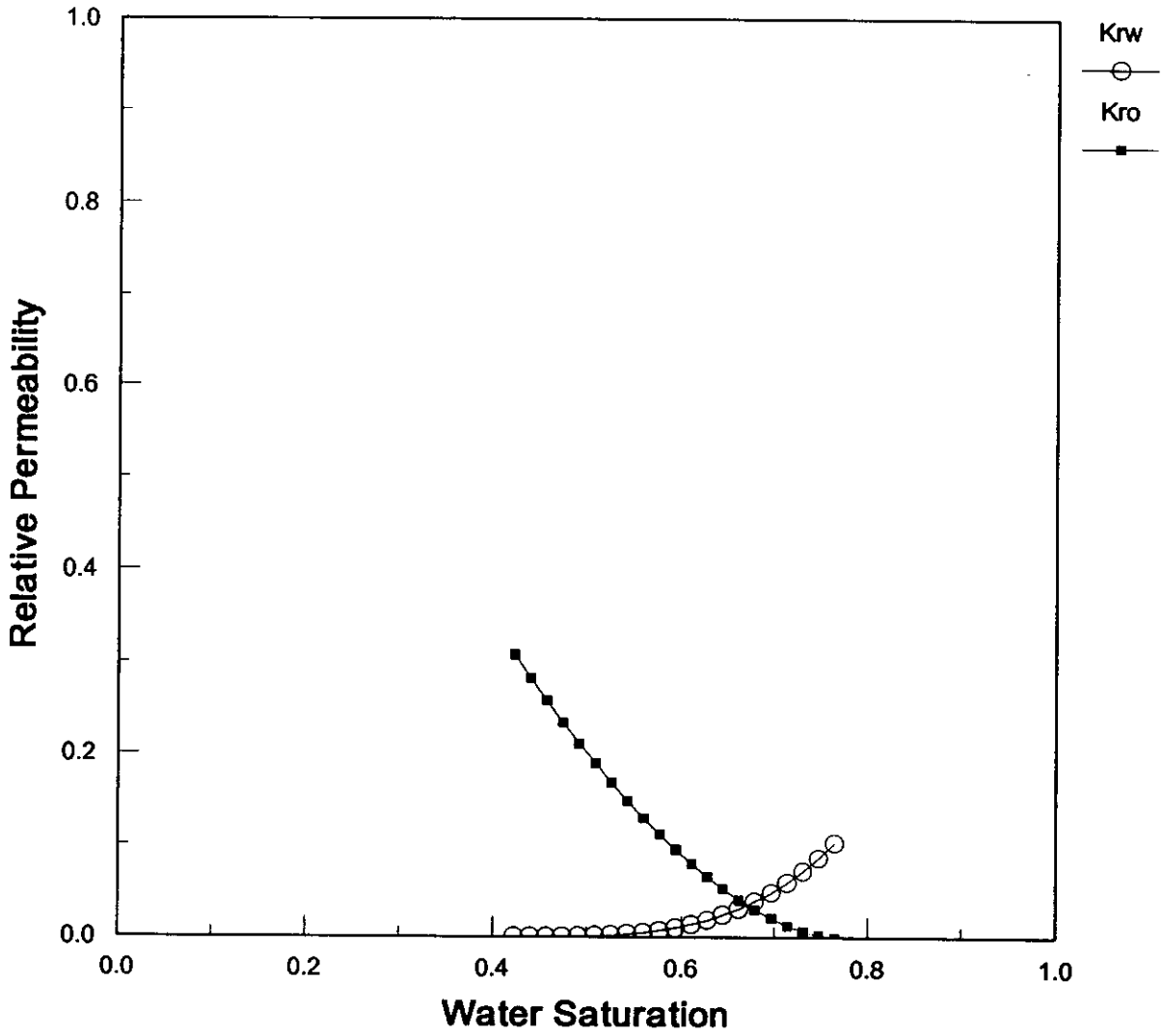

FIGURE 5
TUNDRA - GOODLANDS
RELATIVE PERMEABILITY STUDY
CORE STACK #1 - WATER-OIL RELATIVE PERMEABILITY
RELATIVE PERMEABILITY vs WATER SATURATION

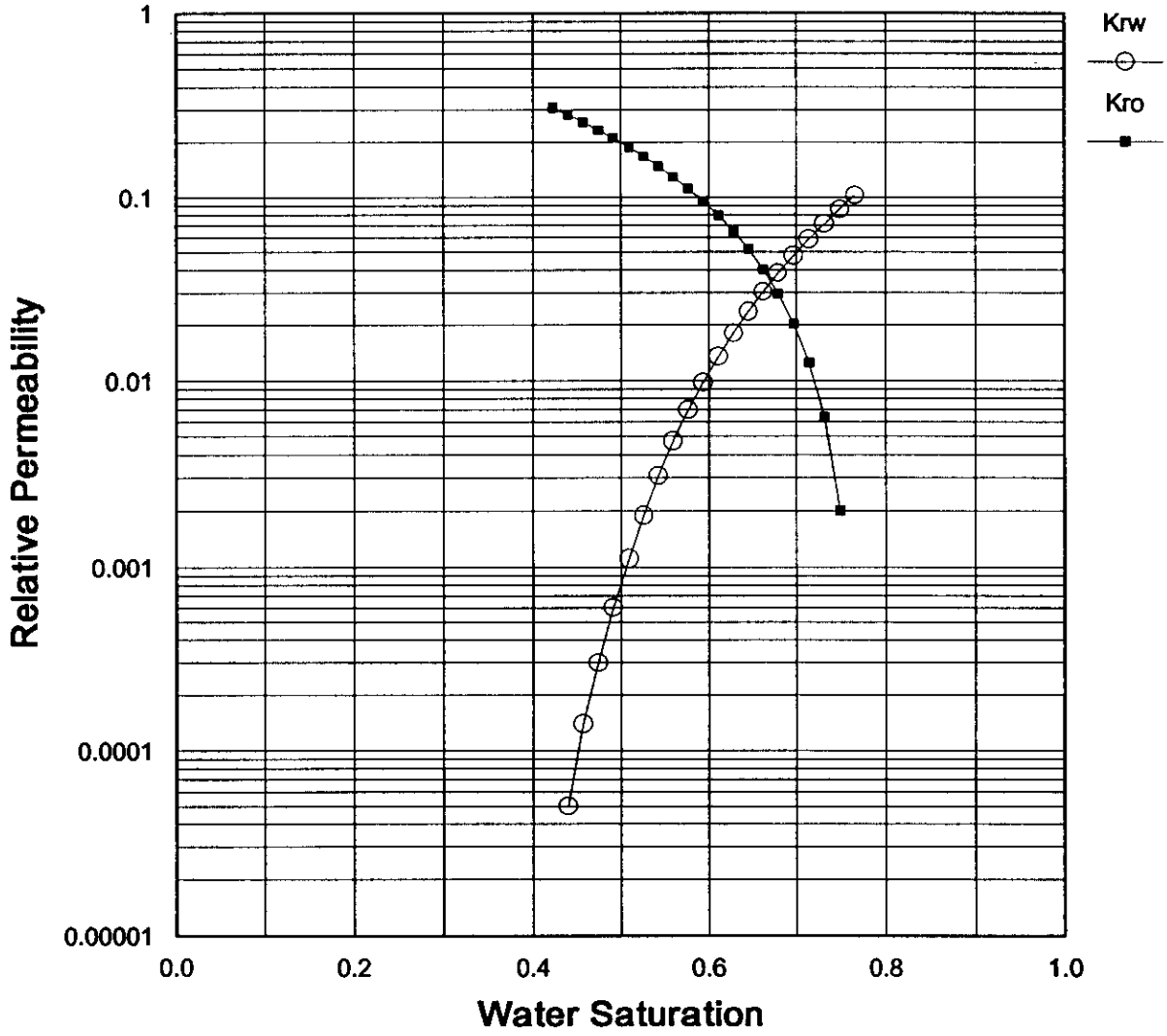

APPENDICES

APPENDIX "A"

RECENT IMPROVEMENTS IN EXPERIMENTAL AND ANALYTICAL TECHNIQUES FOR THE DETERMINATION OF RELATIVE PERMEABILITY DATA FROM UNSTEADY STATE FLOW EXPERIMENTS

D.B.Bennion, Hycal Energy Research Laboratories Ltd.
F.B. Thomas, Hycal Energy Research Laboratories Ltd.

This paper was prepared for presentation at the SPE 10th Technical Conference and Exposition held in Port of Spain, Trinidad, June 26 - 28, 1991.

Summary. Accurate relative permeability data is an essential input parameter for many reservoir engineering applications, most significantly in the area of reservoir simulation. Methods of relative permeability determination are discussed with specific emphasis being given to the calculation of relative permeability curves from unsteady state displacement experiments. Recent advances in history matching techniques for the computation of relative permeability data from unsteady state displacement tests, including rigorous modeling of capillary effects, more flexible cubic and B spline functional forms for the relative permeability relations, and the simultaneous prediction of relative permeability and capillary pressure, are all discussed. Simple corrective techniques for correcting endpoint relative permeability values for in-situ capillary effects are also presented.

Introduction

Relative permeability is an empirical parameter used to modify Darcy's single phase flow equation to account for the numerous complex effects associated with the flow of multiple immiscible phases within porous media[1].

Relative permeability measurements are utilized extensively in many areas of reservoir engineering, and more particularly in recent years in the area of matching, predicting and optimizing reservoir performance and depletion strategies through the use of detailed numerical simulation models.

Those involved in numerical simulation realize the importance of good relative permeability data on the performance of reservoir simulation models. This paper discusses the evolution of relative permeability measurement techniques and reviews the current state of the art technology in the determination of relative permeability data. Recent experimental work and techniques for improving the acquisition of raw laboratory data for relative permeability calculations are also discussed.

Factors Affecting Relative Permeability

Relative permeability can be affected by many physical parameters including fluid saturations,[2-4] physical rock properties,[5-7] wettability,[8-10] saturation history (hysteresis effects),[11,12] overburden stress,[13,14] clay and fines content,[15,16] temperature,[17,18] interfacial tension,[19] viscosity,[20] magnitude of initial phase saturations,[21,22] immobile or trapped phases,[21,22] and displacement rates and capillary outlet phenomena.[23-26] A detailed discussion of the many factors affecting relative permeability is beyond the scope of this paper, but the general consensus of researchers is that in order to obtain the most representative relative permeability data that reservoir conditions during the tests be duplicated as closely as possible. This involves the use of well preserved or restored state reservoir core material, the use of "live" uncontaminated actual reservoir fluids in the tests, and operation at full reservoir conditions of temperature, pressure and confining overburden stress.

Types of Relative Permeability Measurements

A number of researchers have postulated different methods for the experimental determination of relative permeabilities on reservoir core samples. The most popular of these fall into the category of "steady state" and "unsteady state" displacement tests. A number of centrifuge methods have also been proposed[27,28] but in general have had limited acceptance due to the small size of the core samples which can be utilized and the inability to conduct those types of tests at reservoir conditions of temperature and pressure.

Steady State Measurements

Figure 1 provides an illustrative schematic of a typical steady state relative permeability apparatus.

In this type of test a fixed ratio of two or more immiscible fluids are simultaneously forced through a test sample until saturation and pressure equilibrium are established. The experiments are designed in such a way as to eliminate end effects. This is accomplished in a number of ways, the most common being the inclusion of an additional length of core or sandpack to the end of the test section of interest to absorb the capillary end effect. Various other methods such as the use of semi-permeable membranes and plates, or cone shaped core ends to increase production velocity at the outlet face to minimize the end effect, have also been investigated.

At each equilibrium point, in a steady state test, individual-phase permeabilities and relative permeabilities are computed based on the measured phase differential pressures and individual phase flow rates. Once one set of stable data is obtained the injection ratio of the two fluids is varied, stability is re-established and the relative permeabilities at the next saturation level are then determined.

The steady-state method is preferred by some investigators since end effects are negated and, since the test is not truly a displacement test but rather an equilibrium flow test, stability and rate effects associated with viscous instabilities are eliminated. The disadvantages of this method are:

1. Accurate determination of in-situ saturations is required after each displacement level which can be difficult and expensive in reservoir condition tests.

2. Days or weeks are often required to achieve equilibrium at each saturation point. This can result in weeks or months being required to complete a simple relative permeability determination at an extremely high cost.

3. A considerable amount of expensive experimental equipment is required to conduct these tests, particularly at conditions of elevated temperature and pressure.

Unsteady State Measurements

These much simpler tests are conducted rapidly by the displacement of a single phase through a core which is initially saturated with wetting and non-wetting phase and is at the minimum saturation of the phase to be injected (ie. S_{wi} for a waterflood in a water-wet core). The production history and pressure differential across the core are closely monitored during the displacement. Mathematical derivations of classical Buckley-Leverett[29] theory or more complex computer simulation techniques, (which shall be discussed shortly), can be used with this data to compute the relative permeability curves. Because this type of experiment can be conducted relatively rapidly and at a low cost, it is almost exclusively utilized in preference to the steady-state method for commercial relative permeability testing. The main disadvantages of this method are its susceptibility to end effects, rate-dependent instability effects, and potential non-equilibrium between displacing and displaced fluids.

Calculation Methods for Computation of Relative Permeability From Laboratory Data

Steady-State Methods

As discussed previously, relative permeabilities can be computed directly from two-phase steady-state relative permeability displacement tests at given saturation levels. This is a distinct advantage of the steady-state method as no special treatment or manipulation of the data is required. Due to the cost and complexity of steady state measurements; however, they are not often utilized with preference being given to the much simpler

and less expensive unsteady state test.

Unsteady-State Methods

The fluid theory initially described by Buckley and Leverett[29] to describe fluid flow through porous media was later modified by Welge[30] to facilitate the prediction of relative permeability ratios at given saturation levels in laboratory scale core displacement tests. These classical flow equations are described in detail in the above references, to which the reader is referred.

For the case of horizontal flow and negligible capillary pressure, Welge illustrated that:

$$S_{w,av} - S_{w,2} = F_{o_2} Q_w \qquad (1)$$

where:

$S_{w,av}$ = average core water saturation
$S_{w,2}$ = outlet-face water saturation
Fo_2 = fractional flow of oil at outlet face
Q_w = total pore volumes of water injected

Since $S_{w,av}$ and Q_w are known (from material balance and injection data respectively) and Fo_2 can be determined from a plot of Q_w as a function of $S_{w,av}$ it can be calculated that:

$$f_{o_2} = \frac{1}{1 + \frac{\mu_o / k_{ro}}{\mu_w / k_{rw}}} \qquad (2)$$

where:

μ_o, μ_w - oil and water viscosities (cP)
k_{ro}, k_{rw} - endpoint oil and water relative permeability values.

This allows the relative permeability ratio to be computed at any saturation AFTER breakthrough of the water phase. Similar equations can be derived for gas-oil systems.

The work of Welge was extended by Johnson *et al*[31] to obtain a method (commonly called the JBN method) for calculating individual-phase relative permeabilities from unsteady-state test data. These equations are:

$$k_{ro} = \frac{f_{o_2}}{d\left(\frac{1}{Q_w I_r}\right) / d\left(\frac{I}{Q_w}\right)} \qquad (3)$$

$$k_{rw} = \frac{f_{w2}}{f_{02}} \frac{\mu_w}{\mu_o} k_{ro} \qquad (4)$$

$$I_r = \frac{injectivity}{initial\ injectivity} = \frac{Q_{wi} / \Delta P}{(Q_{wi} / \Delta P)_{init}} \qquad (5)$$

where:

F_{w2} = outlet fractional flow of water
ΔP = pressure differential across sample

The advantage of the JBN method over that of the Welge method was that for the first time individual phase relative permeabilities could be computed from unsteady state data instead of merely relative permeability ratios.

The JBN method has been popular since its inception, even though it suffers from some basic deficiencies, and is still used in many applications today.

Another fairly popular method is that of Jones and Roszelle[32]. This method is an extension of the JBN method and also utilizes graphical techniques (which can be computerized).

The basic assumptions of the Jones-Roszelle method are similar to that of the previously discussed JBN method. In this technique the oil produced is expressed as a change in the average water saturation within a core sample. The change in saturation is plotted vs the pore volumes of water injected to calculate the relative permeability ratios

as a function of the water saturation.

The Jones-Roszelle method has particular application late in waterfloods when oil production is very minimal and the slope of the oil recovery vs PV of injection graph becomes very slight. The methods involve plotting recovery vs the inverse of cumulative injection ($1/Q_{wi}$) which avoids long tangent extrapolations back to the y axis and also facilitates easy extrapolation back to the point of infinite water injection ($1/Q_{wi} = O$), which is thought by the authors to yield a better estimation of the true residual oil saturation after a waterflood.

Since all three methods discussed previously are based upon the same fundamental derivations of Buckley-Leveritt flow theory, they tend to be subject to the same limitations, namely:

1. All methods neglect both capillary pressure and gravitational effects in their basic derivation. This means that the methods cannot account for end effect phenomena and the dispersing effect of capillary pressure on saturation shock fronts within porous media. Typically in the past these types of tests were run at very high displacement velocities to yield a large pressure drop across the core sample to minimize the contribution of capillary pressure effects. This can lead to severe problems with both fines mobilization and viscous instability effects.

2. The Welge, JBN and Jones-Roszelle methods all assume perfectly dispersed flow with no core heterogeneities. Since these methods are based on the evaluation of derivatives of the fractional flow curves, if the fractional flow data is non-monotonic, which can often occur in heterogeneous core samples, this results in severe deviations in the computed relative permeability data. This phenomena is illustrated by Sigmund *et al*[33] and appears as Figure 3.

3. Since all of the methods are based upon the analysis of fractional flow data, they can only predict relative permeability data after water breakthrough. In strongly water wet core material, a water displacement results in an almost piston like flow of water through the core resulting in a very steep and localized region of fractional flow. This, therefore, results in only a very small cluster of relative permeability data points being obtained at saturations near the maximum level. Thus significant extrapolation is required for the relative permeabilities at intermediate saturation levels.

This last deficiency was commonly remediated by utilizing a viscous mineral oil in place of the hydrocarbon phase in the test. This, however, yields an improper viscosity ratio which can affect residual saturations and endpoint relative permeability values. Also, the use of refined or synthetic oils can affect core wettability due to the solubilization of asphaltic and heavy ends into solution and cause significant changes in the configuration of the resulting relative permeability curves.

The drawback of the previous three calculation methods is that, since classical behavior is assumed in the method derivations (i.e., no capillary pressure, no end effects, perfectly dispersed flow with no heterogeneities), the accuracy of the obtained relative permeabilities can, in many instances, be questionable.

The implicit history matching technique, first proposed by Archer and Wong[34] is an offshoot of the large advances recently made in reservoir simulation. The basis of the method is that, instead of using known relative permeability relationships in the solution of the partial differential equations which describe multi-phase flow in porous media to predict the pressure and production history, the pressure and production history is utilized to predict the relative permeability curves for a given system.

The method begins by assuming certain functional relationships in the simulator for the wetting and non-wetting phase relative permeabilities and the capillary pressure functions. Initial estimates for adjustable parameters in these equations result in a certain production and pressure history being predicted. This production and pressure history is then compared to the input experimental lab data and the least-square error computed. Correction algorithms adjust the parameters in the functional relationships and the process continues to iterate in this fashion until the minimum least-square error is obtained. The resulting relative permeability curves obtained provide the best fit (within the

limits set by the form of the functional relationships utilized) to the experimental data.

Since the numerical model can incorporate both gravity and capillary pressure effects, these can be incorporated directly into the simulation thus allowing the end effect to actually be simulated as a portion of the experiment. This facilitates running tests at low advance rates to eliminate stability problems. The method also provides a complete history match over the entire range of the saturation change, regardless of the fractional flow characteristics of the displacement, giving it specific application to heterogeneous and strongly wetted systems.

The first published applications of the method were presented by Sigmund and McCaffery.[33] They utilized relatively simple exponential formulations to define the functional form for the relative permeability curves as follows:

$$k_{rw} = k_{rwo}\left[\frac{(Se)^{\epsilon w} + ASe}{1 + A}\right] \qquad (6)$$

$$k_{rnw} = k_{rnwo}\left[\frac{(1-Se)^{\epsilon n} + B(1-Se)}{1 + B}\right] \qquad (7)$$

$$Se = \frac{Sw - Swmin}{Swmax - Swmin} \qquad (8)$$

where:

k_{rw} = Predicted wetting phase relative permeability
k_{rwn} = Predicted non-wetting phase relative permeability
k_{rwo} = Wetting phase endpoint relative permeability
k_{rnwo} = Non-wetting phase endpoint relative permeability
ϵ_w = Wetting phase adjustable shape exponent
ϵ_n = Non-wetting phase adjustable shape exponent
A,B = Linearization constants (0.01 in Sigmunds work)
S_e = Normalized wetting phase saturation
S_w = Wetting phase saturation
S_{wmin} = Minimum wetting phase saturation
S_{wmax} = Maximum wetting phase saturation

Capillary pressure effects were expressed by:

$$P_c = P_{cb}\left[\frac{1}{(S_{pc})^{1/\lambda}} - 1\right] \qquad (9)$$

where:

$$Sp_c = \frac{S_w - S_{wi}}{S_{wo} - S_{wi}} \qquad (10)$$

P_c = Capillary pressure
P_{cb} = Measure of interfacial tension and mean pore size
λ = Pore size distribution parameter
S_{pc} = Normalized capillary pressure saturation value
S_{wi} = Irreducible wetting phase saturation from a drainage capillary pressure test. (Always must be less the S_{wmin}).
S_{wo} = Maximum value of wetting phase saturation corresponding to zero capillary pressure.

The numerical model utilized to match the data incorporated the one-dimensional Buckley-Leverett, incompressible, two phase flow equations;

$$\frac{k}{\mu_w}\frac{\partial}{\partial x}\left(k_{rw}\frac{\partial P_w}{\partial x}\right) = \phi\frac{\partial Sw}{\partial t} + q_{iw} \qquad (11)$$

$$\frac{k}{\mu_{nw}}\frac{\partial}{\partial x}\left(k_{rnw}\frac{\partial P_{nw}}{\partial x}\right) = -\phi\frac{\partial Sw}{\partial t} + q_{nw} \qquad (12)$$

$$P_c = P_{nw} - P_w \qquad (13)$$

where:

k	=	Absolute permeability
μ_w, μ_n	=	Viscosities of wetting and non-wetting phases
k_{rw}, k_{rnw}	=	Relative permeabilities of wetting and non wetting phases
P_w, P_{nw}	=	Pressures in the wetting and non wetting phases
ϕ	=	Porosity
S_w	=	Wetting phase fraction
q_{iw}, q_{nw}	=	Source terms for wetting and non wetting phases
P_c	=	Capillary pressure
∂_x	=	Space co-ordinate
∂_t	=	Time co-ordinate

The model utilized by Sigumund et al utilized one-point upstream transmissibility weighting with linearized implicit transmissibilities (utilizing a secant method to estimate the derivatives) and a modified Newtons method to handle capillary pressure induced non linearities. A 40 gridblock one dimensional model was utilized.

The optimum relative permeability parameters were calculated using a least squares Gauss-Newton optimization routine. The error equation for the i_{th} observation in this routine can be written as:

$$Error = \Delta P^{q}_{OBC_i} + \Delta E^{q}_{OBC_i} \qquad (14)$$

where:

$$\Delta P^{q}_{OBC_i}(\epsilon_w, \epsilon_{nw}) = W_i\left(\Delta P^{obs}_{D_i} - \Delta P^{Calc}_{D_i}\right) \qquad (15)$$

and

$$\Delta E^{q}_{OBC_i}(\epsilon_w, \epsilon_{nw}) = W_i\left(E^{obs}_{R_i} - E^{calc}_{R_i}\right) \qquad (16)$$

where:

Wi	=	Weighting factor
P_D	=	Pressure data
E_R	=	Recovery data
obs	=	Measured data
calc	=	Calculated data
obc	=	objective function

For a given set of "m" observations (data points) the algorithm attempts to find the values of ϵ_w and ϵ_{nw} which will minimize the error function:

$$E = \sum_{i=1}^{m}\left(\left(\Delta P^{q}_{OBC_i}\right)^2 + \left(\Delta E^{q}_{OBC_i}\right)^2\right) \qquad (17)$$

subject to the given constraints;

$$\epsilon_{min} \le \epsilon_w, \ \epsilon_{nw} \le \epsilon_{max}$$

Details of the specific application of the Gauss-Newton correction algorithm can be found in the appendix of Sigmund et al.[33]

Batycky *et al*[24] and MacMillan[35] also utilized this technique using similar functional forms.

One disadvantage of this particular form of the history matching method is that the obtained relative permeability curves can conform to only the configurations possible under the constraints imposed by the given functional form. The exponential forms discussed previously are usually quite adequate for most systems, but cannot adequately model unusual relative permeability configurations, such as those obtained for dual porosity or very heterogeneous systems. Figure 4 provides an illustration of the various types of relative permeability curve configurations which can be obtained using different values of ϵ_w and ϵ_{nw} in the exponential formulation model.

The history matching technique, however, is not limited to the use of any one specific functional relationship. Research by Kerig *et al*[26,37] indicated that free and clamped cubic spline formulations could provide superior fits to almost all types of relative permeability curves.

Kerig *et al* utilized a cubic spline functional form to represent the relative permeability curves defined by:

$$k_{ri} = a_{ij} S_i^3 + b_{ij} S_i^2 + c_{ij} S_i + d_{ij} \qquad (18)$$

For $S_{i,J} \le S_i \le S_{i,J+1}$

Where:

J = number of total spline segments
$S_{i,J}$ = Value of S_i at knot J
$a_{ij}, b_{ij}, c_{ij}, d_{ij}$ = spline coefficients

Cubic splines are highly flexible functions which can, with a sufficient number of spline segments, represent any continuous function as accurately as desired[38]. Figure 5 illustrates the flexibility of cubic splines in modeling relative permeability curves of a nonuniform nature which cannot be well described by simple exponential formulations. Examples of such system would include very heterogeneous reservoirs or systems characterized by multiple porosity types.

Kerig et al[37] discussed sources of error in the relative permeability estimation technique via automatic history matching. They defined two possible sources of error:

1. Modeling Error - Results of inadequacy of the mathematical model of the displacement experiment in the exact representation of the experiment (ie. effect of capillary pressure, heterogeneity or non-uniform initial saturation).

2. Estimation Error

   a) Bias Error - Inability of the functional forms to represent the true, though unknown, relative permeability curves.

   b) Variance Error - errors associated with statistical uncertainty of the data utilized (ie. experimental error) and the number of parameters utilized in the functional form of the relative permeability curves. (Increasing the number of parameters in the functional form generally increases the variance error while reducing the bias error.)

The use of cubic spline formulations over simple exponential formulations can greatly reduce bias error while causing relatively small increases in variance error as illustrated in Figure 6.

Kerig *et al*[39] did additional work in this area and determined specific algorithms for the optimization of the many parameters required when cubic splines are utilized as functional forms in the relative permeability relations. The algorithms utilized incorporated inequality constraints to ensure that physically realistic relative permeability curves were maintained throughout the optimization process. The constraints utilized were such to ensure that the relative permeability curves obtained remained convex downward, remained monotonic, and had zero relative permeability at $S_i = 0$. The optimization program utilized in this work was a Gauss-Newton method with a Marquart modification[40,41]. A detailed discussion of the model and operational constraints utilized can be found in Reference 39.

Watson et al[42] further extended this work to include the use of B Splines[38] as functional forms for the relative permeability curves using:

$$k_{ri}(S_i) = \sum_{j=1}^{N_i} C_j^i B_j^m(S_i) \quad i = w, nw \qquad (19)$$

N_i = Dimensions of the Spline
C_j^i = Parameters to be determined

The use of B Splines has an advantage over the use of Cubic Splines in that B Splines are not "piecewise" type polynomial approximations (ie. each spline segment is valid only over a certain saturation interval). B Splines retain a set of independent coefficients over the entire saturation range of interest making them easier to use while still retaining the flexible nature of cubic splines. The algorithms utilized and operational constraints employed during the optimization process are discussed in detail by Watson et al.[42] Figure 7 illustrates the superior nature of spline estimated relative permeability data over that predicted by simple exponential models.

Richmond *et al*[43] further extended the work of Watson *et al*[42] to include simultaneous optimization of capillary pressure data along with the prediction of relative permeabilities from displacement experiments. The functional form for the capillary pressure was also defined by B Splines as:

$$P_c(S_w) = \sum_{J=1}^{N_i} C_J^I B_J^m(S_w) \qquad (20)$$

Richmond *et al*[43] utilized a Levenberg-Marquart Algorithm with linear inequality constraints in their optimization process. They also investigated the problem of convergence on multiple distinct local minima by variation of their initial optimization initialization point and covariance analysis of the Hessian matrix obtained from the solution of the data. Also proposed was a new procedure for the automatic selection of the optimum number and location of the spline knots to obtain the maximum accuracy in estimation with the minimum number of spline segments and resulting optimizations.

The work of Richmond *et al* utilized pure parameter adjustment for the history matching of the capillary pressure functions to optimize the error between the experimentally observed pressure and production history and the simulator predicted data. Recent research at Hycal has been involved in the actual measurement of in-situ capillary pressures during a dynamic displacement test through the use of pressure transducers equipped with special wetted membranes to sense specific individual phase pressures and the resulting capillary pressure.

The measurement of actual dynamic capillary pressure data allows the further extension of the history matching technique to the direct history matching of the capillary pressure curve allowing for the direct prediction of both reservoir condition relative permeabilities and capillary pressures accurately and inexpensively from a single test. Further testing and experimentation is still under way to continue to improve and refine this latest addition to the history matching method.

Simple Correction Techniques for Endpoint Relative Permeability Values

All of the history matching models previously discussed require that the user input both the wetting and non wetting phase endpoint relative permeability values. Relative permeability endpoint values, determined utilizing a standard unsteady state displacement technique, may often result in the measurement of endpoint values which are substantially lower than actual values measured from steady state tests. Figure 8[44] illustrates this phenomena for displacement tests conducted at the same rate utilizing both a Penn-State type steady state approach vs the standard unsteady state test methodology.

The major cause of this type of phenomena is attributed to capillary effects. An excellent discussion of capillary and rate effects can be found in the work of Batycky[24], Osaba[45], and Rapoport and Leas.[46]

Capillary pressure is simply defined as:

$$P_c = P_{nw} - P_w \qquad (21)$$

where:

P_c = Capillary Pressure (kPa or Psi)
P_{nw} = Non-wetting Phase Pressure (kPa or Psi)
P_w = Wetting Phase Pressure (kPa or Psi)

When a single fluid is flowing in the porous media in the presence of other immobile residual immiscible fluid phases (i.e. the flow of water at a residual oil saturation), a certain portion of the applied force to move the fluid through the system is required to overcome the capillary forces which exist within the sample. Generally, the larger the capillary forces which exist within a sample, the larger the influence on the endpoint relative permeability data.

Typically in the past relative permeability tests were conducted at high rates which resulted in a relatively large pressure differential across the core sample which, in general was much larger than the capillary pressure force and thus tended to minimize its overall effect on the measured endpoint relative permeability value. Figure 9[44] provides an illustrative example of this phenomena.

The use of high rates in conducting unsteady state relative permeability tests has associated problems, these being:

1. The potential for fines migration.
2. Unstable flow effects due to viscous instability.[23]

3. Erroneous pressure data due to non-Darcy flow caused by turbulent interstitial flow.

4. Experimental data acquisition difficulties resulting from a very short test time.

Recent work has illustrated that a simple correction technique can be accurately applied to correct for the effect of capillary effects on endpoint relative permeabilities while avoiding many of the aforementioned difficulties. The technique is applied as follows:

1. Conduct a regular, low rate unsteady state displacement test, measure the resulting endpoint relative permeability and residual fluid saturations..

2. Use the computer history matching routine to generate the complete relative permeability curves.

3. Conduct geometric rate increases of the displacing phase at 2 to 3 higher displacement velocities. Example, if the base displacement test was conducted at a rate of 10 ml/hr, conduct additional endpoint tests at 20, 40 and 80 ml/hr. The technique does not require the use of excessively high injection rates and these should be avoided to reduce the potential for fines mobilization or unstable flow.

4. Record any additional production of the residual immobile phase caused by the increase in interstitial fluid shear force.

The profile of the experimental results can have three configurations as illustrated in Figure 10, these being:

CASE 1 - Endpoint permeability remains constant with rate illustrating perfect conformance to Darcies Law indicating an absence of capillary effects. This indicates that no correction of the endpoint relative permeability data is required and that capillary effects are negligible.

CASE 2 - Endpoint permeability increases with increasing injection rate. This indicates the presence of capillary forces, a reduction in the residual immobile phase saturation, or a combination of both phenomena. The endpoint correction technique, to be discussed shortly, should be applied here.

CASE 3 - Endpoint permeability decreases or initially increases then decreases with increasing injection rate. This indicates either damage by fines mobilization or turbulent flow phenomena. These two phenomena can be easily differentiated by reducing to the base rate and observing if the permeability returns to the originally recorded value. In the case of fines migration the endpoint correction technique, in general, can still be applied if sufficient points (3 minimum) are available prior to the reduction in permeability. If turbulent flow occurs, lower rates should be selected to allow evaluation in the laminar flow regime.

The correction technique is applied by fitting the non linear model:

$$k_i = a_1\left(1 - e^{-a_2 q_i}\right) \qquad (22)$$

where: k_i = measured endpoint permeability at flow rate "i" (mD or μm^2)

q_i = flow rate at point "i" (cc/hr, cc/sec)

a_1, a_2 = adjustable constants

to the experimentally determined data. In this work a non-linear finite difference Levenberg-Marquardt optimization routine[41,47-49] was used to optimize the values of the constants a_1 and a_2 to yield the minimum least square error between the experimental and predicted data.

By definition, as the flowrate, q_i approaches infinity, the pressure across the sample also becomes infinitely larger than any contribution associated with capillary effects. Thus,

$$\lim_{q_i \to \infty} a_1\left(1 - e^{-a_2 q_i}\right) = a_1 \qquad (23)$$

Thus the value of the constant a_1 provides the simple final approximation to the final corrected

permeability value. Examples of the application of this technique for both water oil and gas-oil displacement tests appear as Tables 1 and 2 and Figures 11 and 12. The resulting relative permeability data is simply renormalized at this point to the higher endpoint relative permeability value.

If the residual immobile phase saturation is reduced by the elevated rate displacements, as may sometimes occur due to the increase in capillary number associated with the higher displacement velocity. This is accommodated by (See Figure 13):

1. Determine "new" final residual saturation.

2. Using the previously derived and matched functional form for the relative permeability curve, extrapolate the existing relative permeability curve to the "new" residual saturation.

3. Normalize the new set of relative permeability data up to the final corrected endpoint relative permeability.

Use of this technique eliminates the use of high displacement rates during the actual two phase immiscible displacement test which obviates the potential for viscous instability effects. Since the method works upon an extrapolative technique, this also eliminates the need for extreme flow velocities to facilitate the endpoint correction, and thus has specific application to velocity sensitive core materials.

Conclusions

Recent advances in unsteady state displacement technology have allowed the data from these relatively simple and inexpensive tests to have much wider application and improved accuracy when correlated with the data from more expensive and time consuming steady state tests. Advances have been made in automatic history matching, particularly with the advent of more sophisticated cubic spline and B spline functional forms for the relative permeability and capillary pressure relations. Recent work also indicates the possibility of the prediction of accurate reservoir condition capillary pressures simultaneously during unsteady state displacement tests. Simple procedures for the correction of endpoint relative permeability data by the use of parameter estimation techniques to match the results of multirate flow tests were documented and illustrative examples of the technique presented.

References

1. Muskat, M., and Meres.: M.W.: *Physics,* Vol. 7, (1936) 346.

2. Leverett, M.C., and Lewis, W.B.: "Steady Flow of Gas-Oil-Water Mixtures Through Unconsolidated Sands," *Trans.*, AIME, Vol. 142 (1941) 107.

3. Sarem, A.M.: "Three Phase Relative Permeability Measurements by Unsteady State Methods," *SPEJ*, Vol. 9 (1966) 199.

4. Owens, W.W. and Archer, D.E.: "The Effect of Rock Wettability on Oil-Water Relative Permeability Relationships," *Trans.*, AIME (July 1971) 873-78.

5. Maloney, D.R., Honarpour, M.M., Brinkmeyer, A.D.: "The Effects of Rock Characteristics on Relative Permeability," NIPER Report No. FC22-83 FE 60149 (January 1990).

6. Morrow, N.R.: "Capillary Pressure Correlation for Uniformly Wetted Porous Media," *JCPT*, (Oct. 1976).

7. Arps, J.J. and Roberts, T.G.: "The Effect of the Relative Permeability Ratio, the Oil Gravity and the Solution Gas-Oil Ratio on the Primary Recovery from a Depletion Type Reservoir," *Trans.*, AIME Vol. 24 (1955) 120.

8. Craig, F.F., Jr.: "The Reservoir Engineering Aspect of Waterflooding," *SPE Monogram Series* (1971).

9. Wang, F.H.L.: "Effect of Wettability Alteration on Water/Oil Relative Permeability, Dispersion, and Flowable Saturation in Porous Media," *SPE Res. Eng.* (May 1988).

10. Morrow, N.R., Lim, H.T., Ward, J.S.: "Effect of Crude Oil Induced Wettability Changes on Oil Recovery," *SPE Form. Eval.* (Feb. 1986).

11. Geffen, T.M., Owens, W.W., Parrish, D.R., and Morse, R.A.: "Experimental Investigation of Factors Affecting Laboratory Relative Permeability Measurements," *Trans.*, AIME, Vol. 192, (1951) 99.

12. Land, C.S.: "Comparison of Calculated and Experimental Imbibition Relative Permeability," *Trans.*, AIME, Vol. 251 (1971) 419.

13. Wei, K.K., Morrow, N.R., Brower, K.R.: "Effect of Fluid, Confining Pressure and Temperature on Absolute Permeabilities of Low Permeability Sandstones," *SPE Form Eval.* (August 1986).

14. Gobran, B.D., Brigham, W.E., Ramey, J.H. Jr.: "Absolute Permeability as a Function of Confining Pressure, Pore Pressure, and Temperature," *SPE Form. Eval.*, (March 1987).

15. Soeder, D.J.: "Laboratory Drying Procedures and The Permeability of Tight Sandstone Core," *SPE Form. Eval.* (February 1986).

16. Selby, R.J., Ali, S.M.F.: "Mechanics of Sand Production and the Flow of Fines in Porous Media," *JCPT*, (May 1988).

17. Nakornthorp, K., Evans, R.D.: "Temperature Dependant Relative Permeability and Its Effect on Oil Displacement by Thermal Methods," *SPE Res. Eng.*, (May 1986) 230-242.

18. Polikar, M., Ali, S.M.F., Puttagunta, V.R.: "High Temperature Relative Permeabilities For Athabasca Oil Sands," *SPE Res. Eng.* (Feb. 1990).

19. Morrow, N.R., Chatzes, I., Taber, J.J.: "Entrapment and Mobilization of Residual Oil in Bead Packs," *SPE Res. Eng.* (1988).

20. LeFebvre duPrey, E.J.: "Factors Affecting Liquid-Liquid Relative Permeabilities of Consolidated Porous Medium," *SPEJ 2*, (1973) 39.

21. Caudle, B.H., Slobod, R.L., and Brownscombe, E.R.: "Further Developments in the Laboratory Determination of Relative Permeability," *Trans.*, AIME, Vol. 192 (1951) 145.

22. McCaffery, F.G.: "The Effect of Wettability on Relative Permeability and Imbibition in Porous Media," Ph.D. Thesis, University of Calgary, Alberta, Canada (1973).

23. Sigmund, P., Sharma, H., Sheldon, D. and Aziz, K.: "Rate Dependence of Unstable Waterfloods," *SPE Res. Eng.* (May 1988).

24. Batycky, J.P., McCaffery, F.G., Hodgous, P.K. and Fisher, D.B.: "Interpreting Relative Permeability and Wettability from Unsteady State Displacement Measurements," *SPEJ*, (June 1981) 296.

25. Peters, E.J., and Flock, D.L.: "The Onset of Instability During Two-Phase Immiscible Displacement in Porous Media," *SPEJ*, (April 1981) 249.

26. Bentsen, R.G.: "A New Approach to Instability Theory in Porous Media," *SPEJ*, (Oct. 1985) 765.

27. Van Spronsen, E.: "Three-Phase Relative Permeability Measurements Using the Centrifuge Method." Paper SPE/DOE 10688 Presented at the Third Joint Symposium, Tulsa, Okla. (1982).

28. O'Mera, D.J., Jr. and Lease, W.O.: "Multiphase Relative Permeability Measurements Using an Automated Centrifuge," Paper SPE 12128 Presented at the SPE 58th Annual Technical Conference and Exhibition, San Francisco (1983).

29. Buckley, S.E. and Leverett, M.D.: "Mechanism of Fluid Displacement in Sands," *Trans.*, AIME, Vol. 146 (1942) 107.

30. Welge, H.J.: "A Simplified Method for Computing Recovery by Gas or Water Drive," *Trans.*, AIME, Vol. 195 (1952) 91.

31. Johnson, E.F., Bossler, D.P., and Nauman, V.O.: "Calculation of Relative Permeability from Displacement Experiments," *Trans.*, AIME, Vol. 216, 2959, 370.

32. Jones, S.C. and Rozelle, W.O.: "Graphical Techniques for Determining Relative Permeability from Displacement Experiments," *JPT*, Vol. 15 (1978) 807.

33. Sigmund, P.M., and McCaffery, F.G.: "An Improved Unsteady-State Procedure for Determining the Relative Permeability Characteristics of Heterogeneous Porous Media," *SPEJ* (Dec. 1973) 343.

34. Archer, J.S., and Wong, S.W.: "Use of a Reservoir Simulator to Interpret Laboratory Waterflood Data," *SPEJ*, (Dec. 1973) 343.

35. MacMillan, D.J.: "Automatic History Matching of Laboratory Corefloods to Obtain Relative Permeability Curves," *SPERE*, (February 1987) 85.

36. Kerig, P.D.: "Estimation of Relative Permeabilities from Displacement Experiments," PhD. Dissertation, Texas A & M Univ., College Station, Texas (1985).

37. Kerig, P.D., Watson, A.T.: "Relative Permeability Estimation from Displacement Experiments: An Error Analysis," *SPE Res. Eng.* (March 1986).

38. Schumaker, L.L.: *Spline Functions: Basic Theory,* John Wiley and Sons Inc., New York (1981).

39. Kerig, P.D. and Watson, A.T.: "A New Algorithm for Estimating Relative Permeabilities From Displacement Experiments," *SPE Res. Eng.,* (1987).

40. Bard, Y.: *Nonlinear Parameter Estimation*, Academic Press, New York (1974).

41. Marquart, D.W.: "An Algorithm for Least Squares Estimation of Non-Linear Parameters," *Soc. Industrial Applied Math Journal*, (1963).

42. Watson, A.T., Richmond, P.C., Kerig, P.D. and Tao, T.M.: "A Regression Based Method for Estimating Relative Permeabilities from Displacement Experiments," *SPE Res. Eng.* (1988).

43. Richmond, P.C. and Watson, A.T., "Estimation of Multiphase Flow Functions From Displacement Experiments," *SPE Res. Eng.* (1990).

44. Fassihi, M.R., "Estimation of Relative Permeability from Low Rate Unsteady State Tests - A Simulation Approach," *JCPT*, (May 1989).

45. Osaba, J.S.: "Laboratory Measurements of Relative Permeability," *Trans.*, AIME Vol. 192 (1951) 47.

46. Rapoport, L.A., and Leas, W.J.: "Relative Permeability to Liquid in Liquid-Gas Systems," *Trans.*, Vol. 192 (1951).

47. Brown, K.M., and Dennis, J.E.: "Derivative Free Analogues of the Levenberg-Marquardt and Gauss Algorithms for Nonlinear Least Squares Approximations," *Numerische Mathematik*, 18 (1972) 289-297.

48. Brown, K.M.: "Computer Oriented Methods for Fitting Tabular Data in the Linear and Nonlinear Least Squares Sense," Department of Computer, Information, and Control Sciences, TR No. 72-13, University of Minnesota.

49. Levenberg, K.: "A Method for the Solution of Certain Non-Linear Problems in Least Squares," *Quart. Appl. Math.* 1, (1944) 164-168.

TABLE 1
CORE AND FLUID PARAMETERS
FOR ENDPOINT CORRECTION TESTS

	Core "A"	Core "B"
Length (cm)	5.45	4.85
Diameter (cm)	3.80	3.80
Porosity (%)	21.0	17.2
Water Viscosity (cP)	0.581	0.581
Live Oil Viscosity (cP)	3.78	3.78
Gas Viscosity (cP)	0.0124	0.0124

TABLE 2
ENDPOINT CORRECTION TEST DATA

CORE "A"			
Injection Rate (ml/hr)	Endpoint Permeability To Water (mD)	Injection Rate (ml/hr)	Endpoint Permeability To Gas (mD)
10	1.85	20	0.825
20	2.37	50	2.79
50	4.07	100	3.56
100	6.82	200	4.69
200	10.98	500	7.69
Extrapolated Endpoint Permeability	14.50		7.92
CORE "B"			
Injection Rate (ml/hr)	Endpoint Permeability To Water (mD)	Injection Rate (ml/hr)	Endpoint Permeability To Gas (mD)
5	2.55	10	3.61
20	4.43	20	7.10
40	6.62	50	9.35
80	9.59	100	9.90
200	13.17		
Extrapolated Endpoint Permeability	13.27		10.03

Figure 1 - Steady State Relative Permeability Apparatus

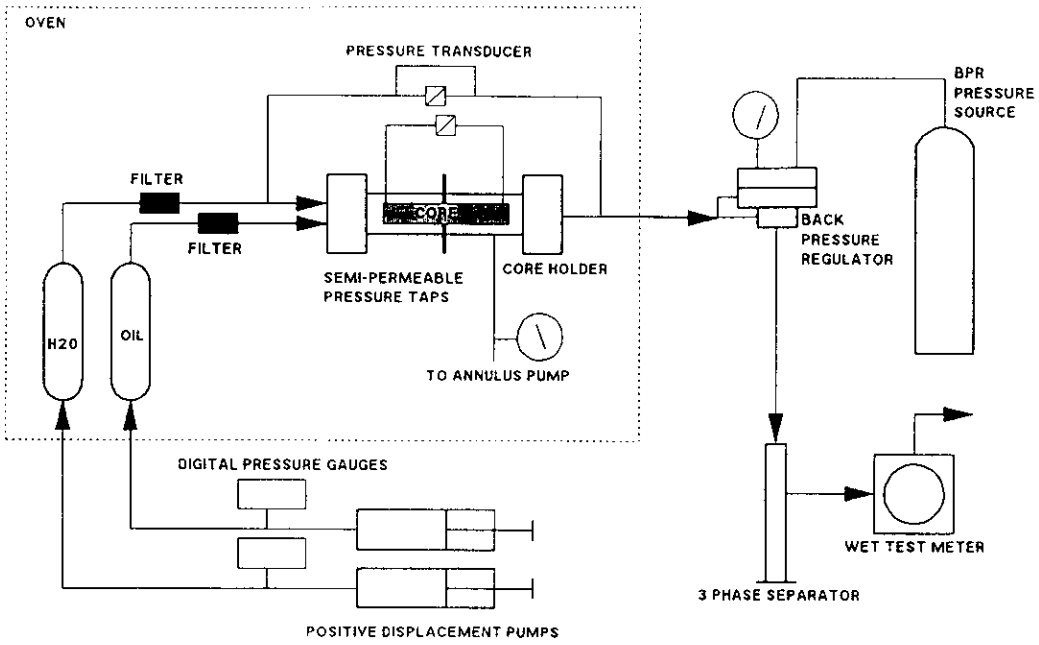

Figure 2 - Unsteady State Relative Permeability Apparatus

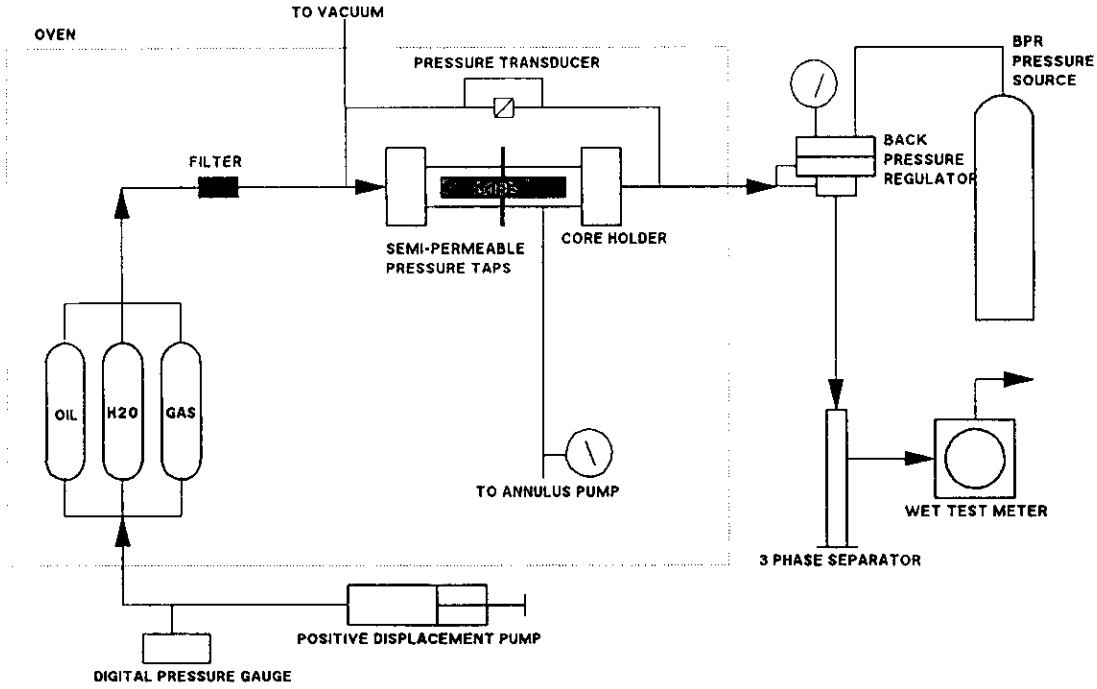

FIGURE 3

IMBIBITION RELATIVE PERMEABILITY - JBN METHOD
RELATIVE PERMEABILITY vs
NORMALIZED WETTING PHASE SATURATION FRACTION

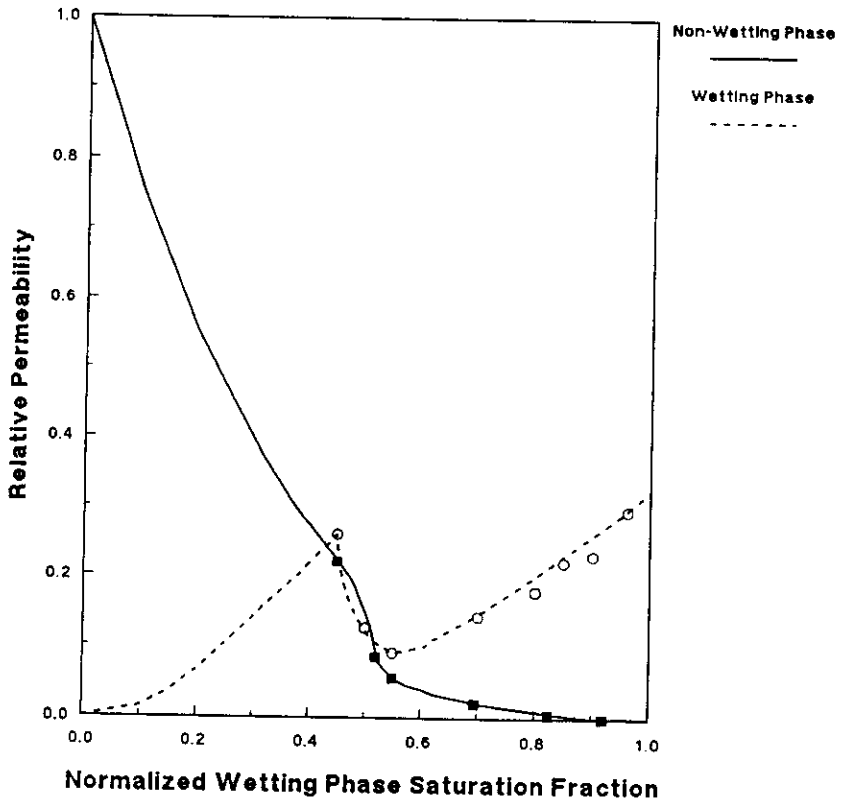

From Sigmund et al (Ref 33)

FIGURE 4

COMPARISON OF VARIOUS RELATIVE PERMEABILITY
CURVE CONFIGURATIONS USING EXPONENTIAL
FUNCTIONAL FORMS

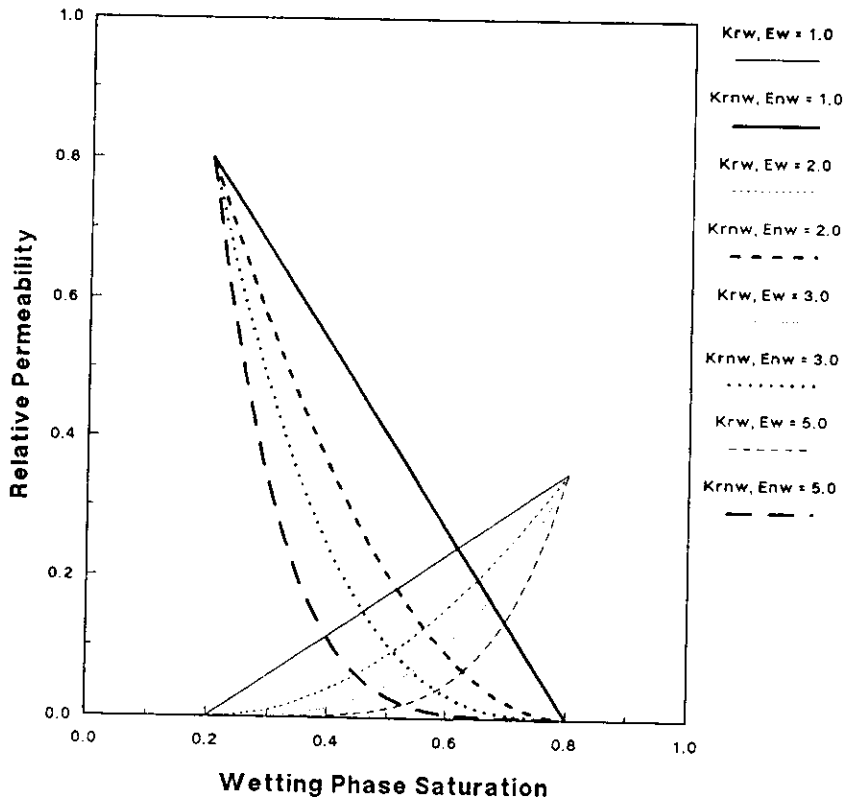

FIGURE 5

EXAMPLE OF RELATIVE PERMEABILITY CURVE CONFIGURATIONS GENERATED USING CUBIC SPLINE FUNCTIONAL FORMS

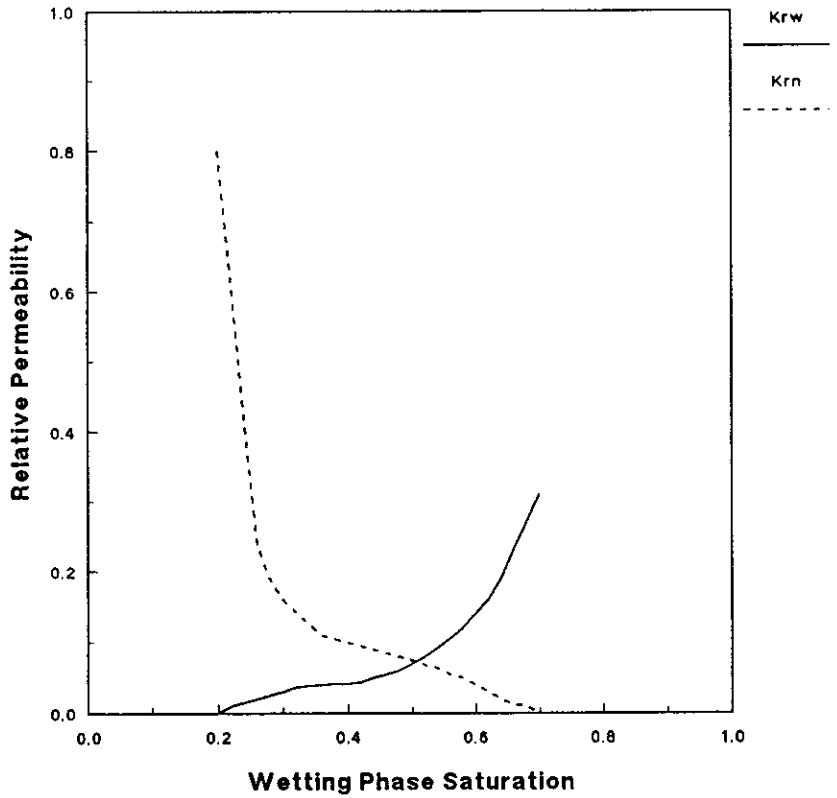

FIGURE 6

ILLUSTRATION OF BIAS ERROR ASSOCIATED WITH THE USE OF EXPONENTIAL FUNCTIONAL FORMS FOR RELATIVE PERMEABILITIES IN AUTOMATIC HISTORY MATCHING

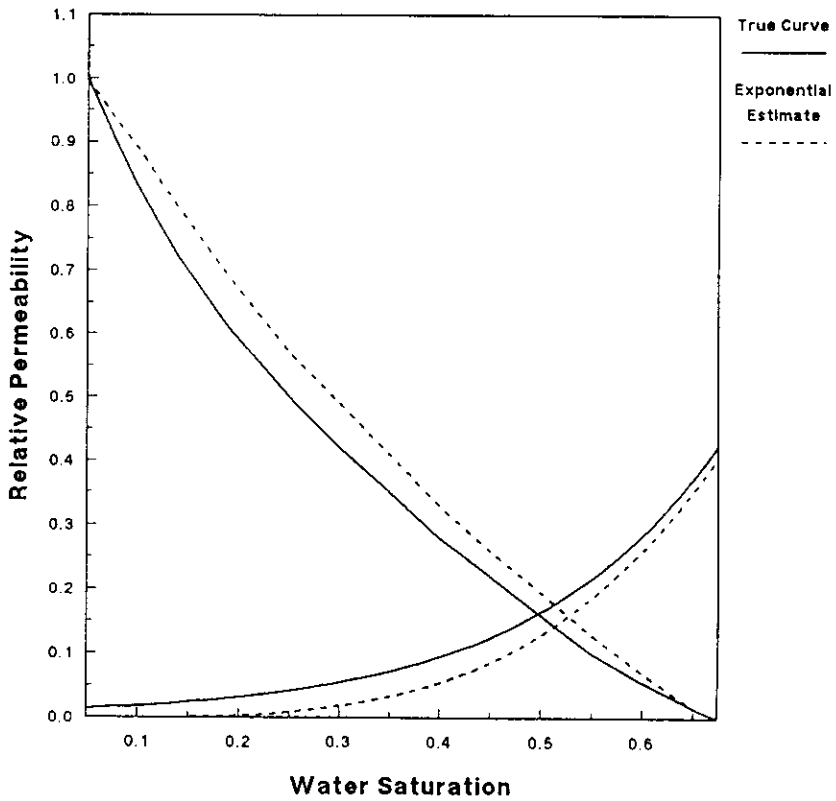

From Kerig et al (Ref 37)

FIGURE 7

COMPARISON OF EXPONENTIAL AND SPLINE FUNCTIONAL FORMS FOR GENERATING RELATIVE PERMEABILITY CURVES BY THE AUTOMATIC HISTORY MATCHING METHOD

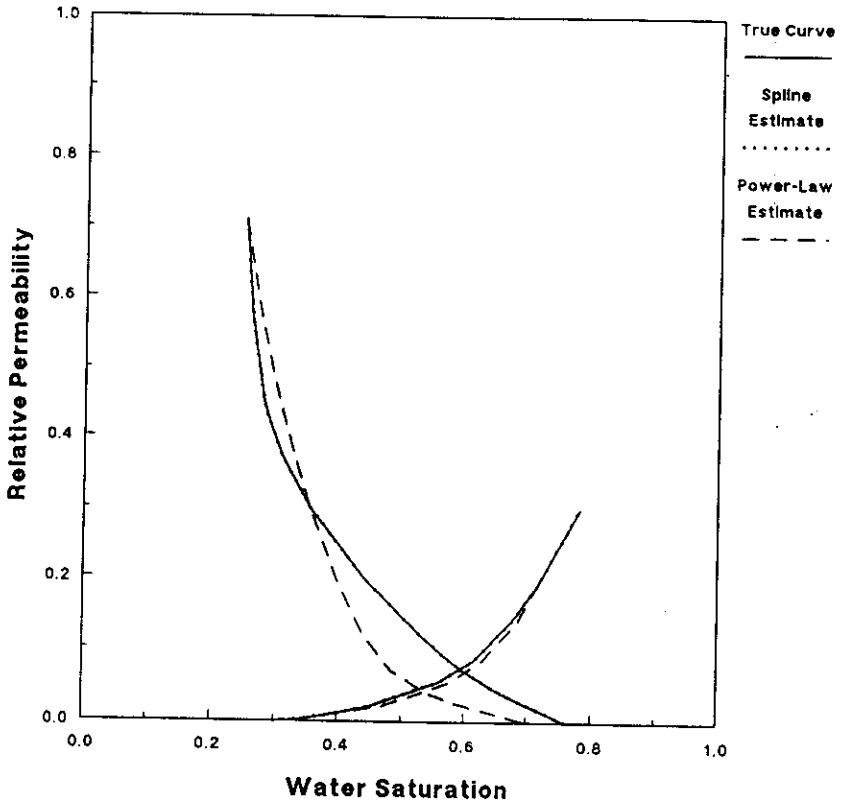

From Watson et al (Ref 42)

FIGURE 8

EFFECT OF AN OUTLET SECTION IN NEGATING CAPILLARY END EFFECT

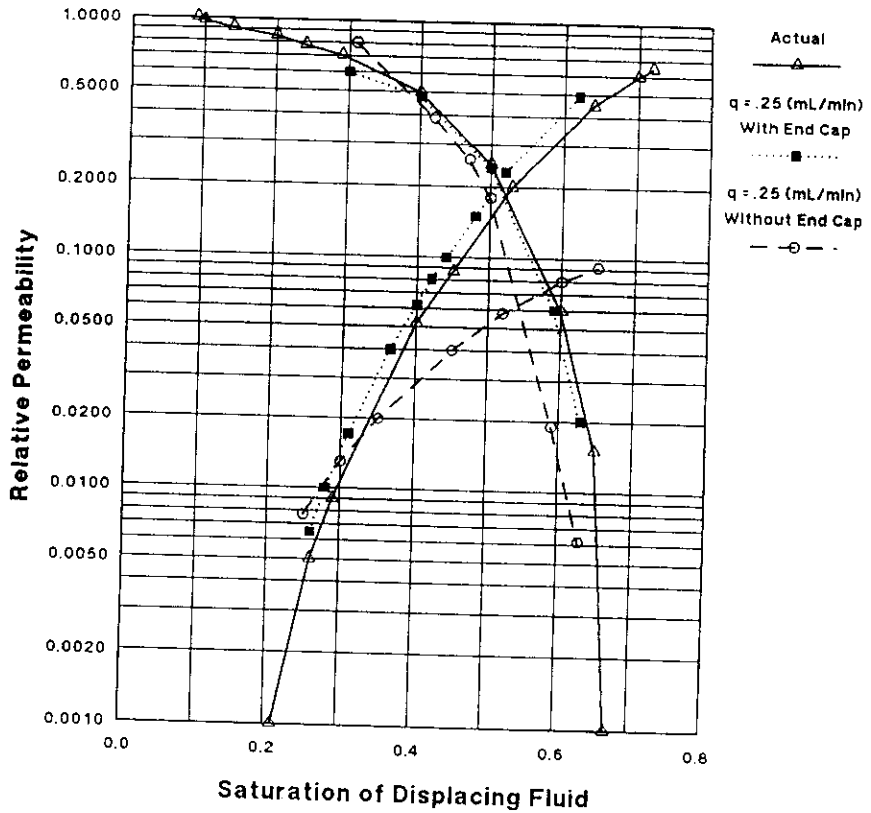

From Fassihi (Ref 44)

FIGURE 9

EFFECT OF RATE IN NEGATING CAPILLARY END EFFECTS

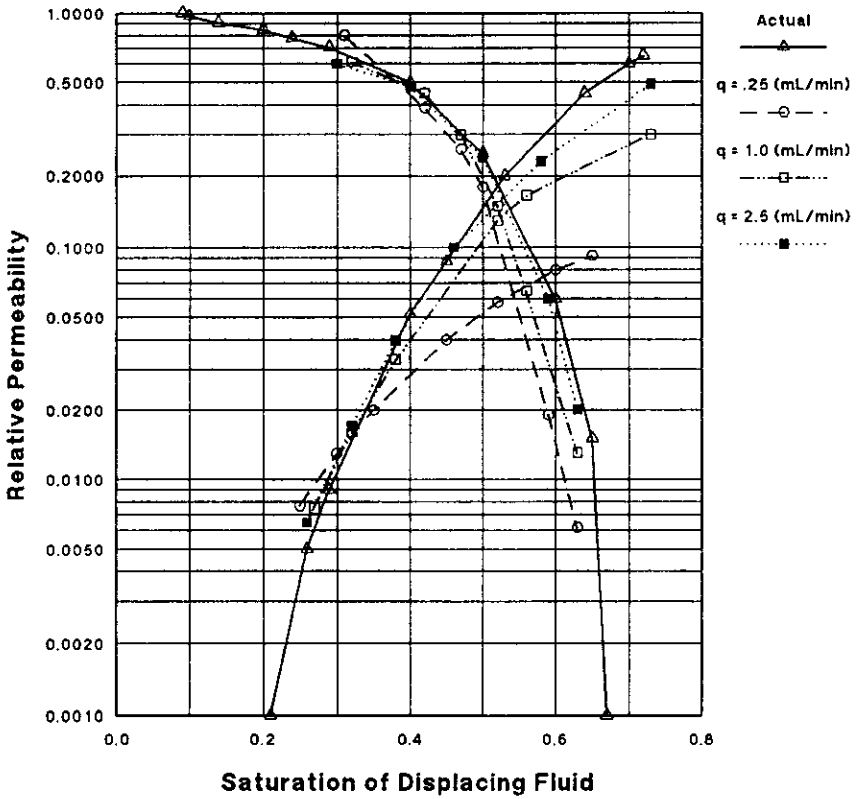

From Fassihi (Ref 44)

FIGURE 10

ILLUSTRATION OF POTENTIAL CONFIGURATIONS OF PERMEABILITY PROFILES FROM ELEVATED RATE DISPLACEMENT TESTS FOR ENDPOINT CORRECTION

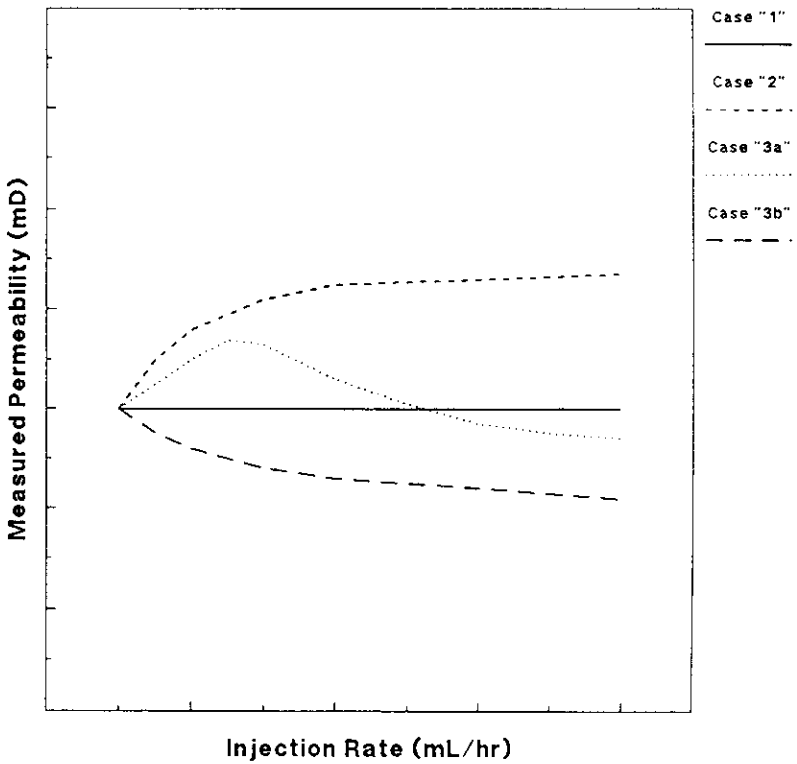

FIGURE 11
ENDPOINT CORRECTION TEST DATA
WATER-OIL TESTS

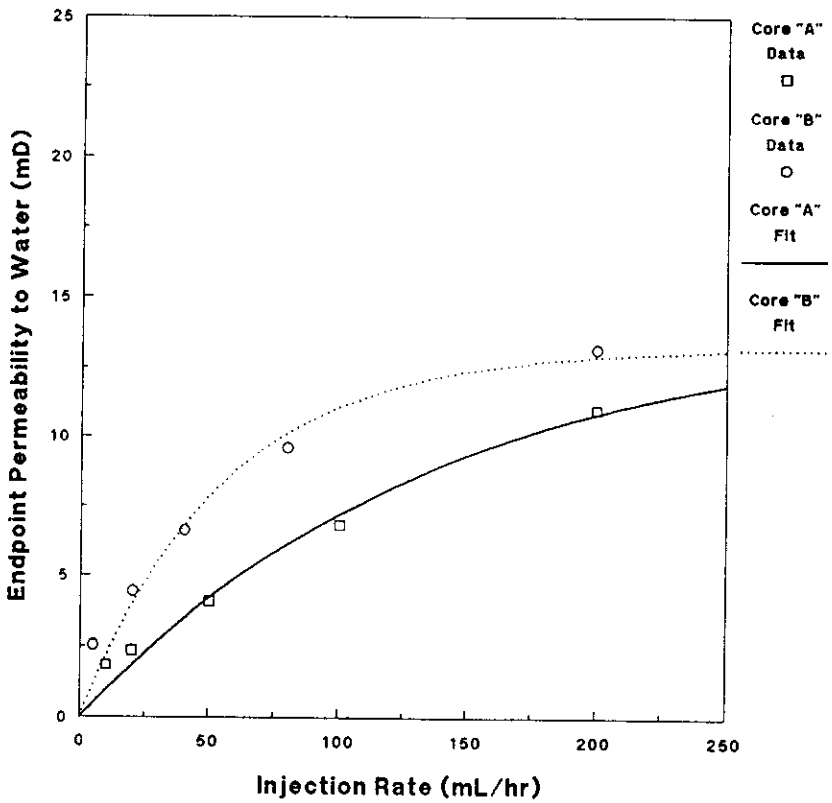

FIGURE 12
ENDPOINT CORRECTION TEST DATA
GAS-OIL TESTS

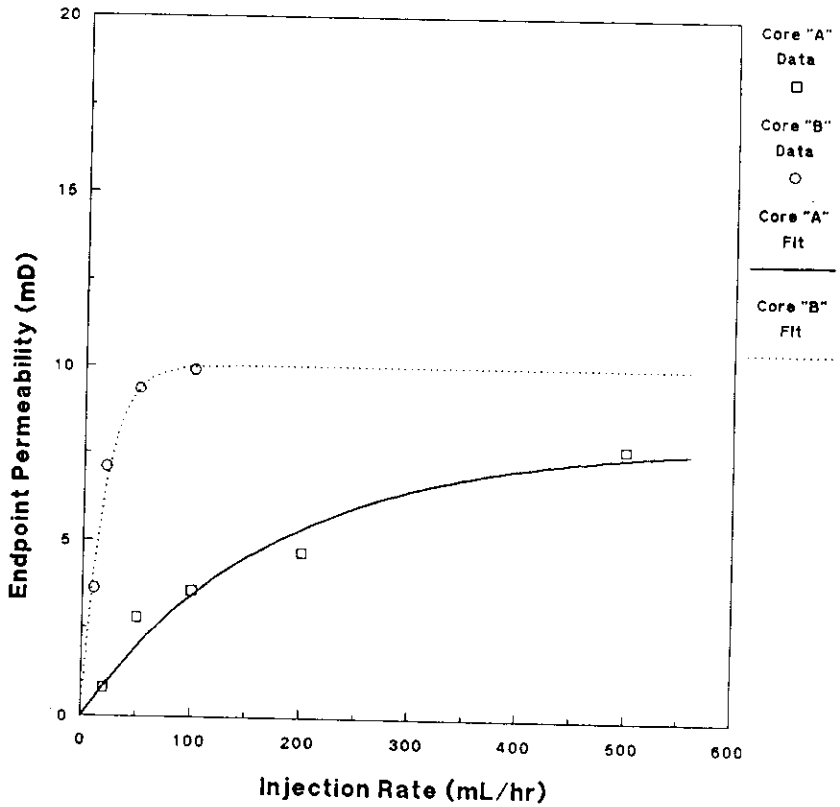

FIGURE 13
EXAMPLE OF APPLICATION OF ENDPOINT CORRECTION METHOD FOR THE CASE OF A CHANGE IN ENDOINT RESIDUAL SATURATION

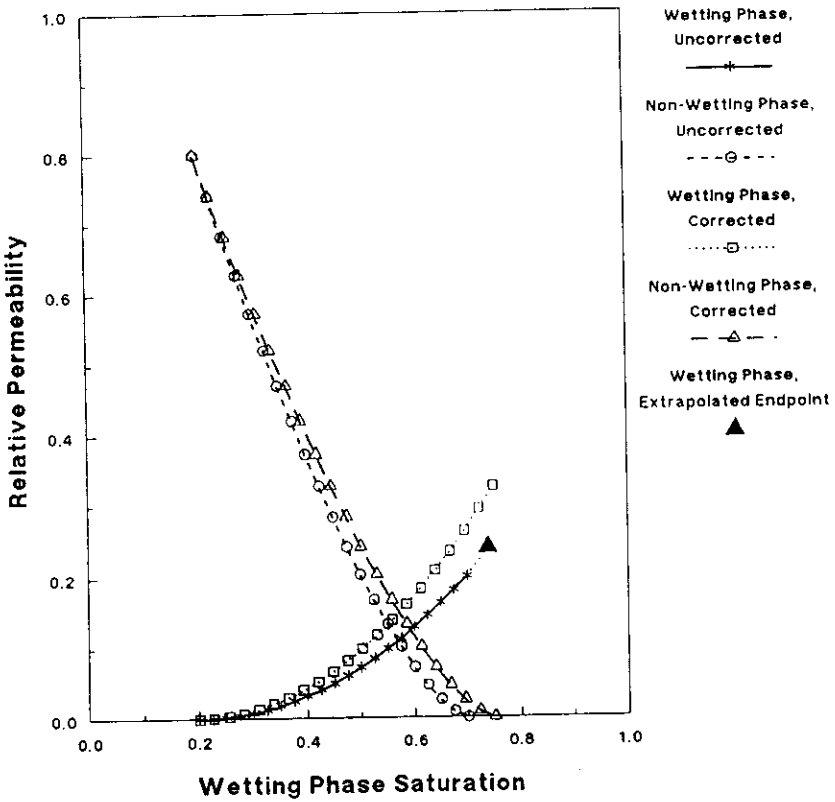

DISKETTES

DATA DISKETTE

Tundra oil and gas ltd.

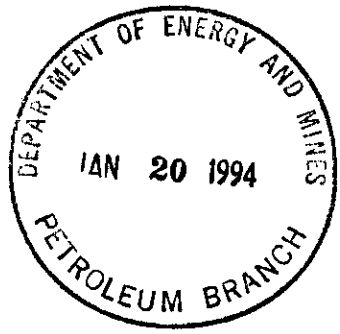

January 18, 1994

FILE : FIELD & POOL FILE
OTHER AREAS
LOWER AMARANTH I POOL
SPECIAL CORE STUDY

Manitoba Energy and Mines
Petroleum Branch
555 - 330 Graham Avenue
Winnipeg, MB
R3C 4E3

Attention: John Fox

Dear John:

RE: University of Manitoba Advanced Petroleum Geology Project

On behalf of Ms. Lisa Sack, and in accordance with our letter of September 17, 1993, I am providing the Branch with two copies of Ms. Sack's final written report on the Goodlands core study. Tundra would like to acknowledge the support of the Branch and the assistance of the staff of the Core Centre.

The report adds to the body of knowledge with respect to the Spearfish as a reservoir and complements those reports prepared by commercial sources. Further, it broadens the geographic area over which the Spearfish reservoir petrography has been studied in detail. Should you or any of your staff have questions with regard to Ms. Sack's work, I suggest you contact her directly at the University of Manitoba.

Sincerely,

TUNDRA OIL AND GAS LTD.

C. Mike Finn, P. Geol.
Chief Geologist

CMF/bp

cc Bill Last, University of Manitoba
Lisa Sack, University of Manitoba

1111 - One Lombard Place, Winnipeg, Manitoba R3B 0X4 Telephone: (204) 934-5850 Fax: (204) 934-5820

REPORT

7.747 Advanced Petroleum Geology & Geochemistry

Lisa Sack

INTRODUCTION

The objectives of this project were to analyze the Lower Amaranth Formation samples from Tundra wells 6-11-24 W1 and 4-14-1-24 W1 to: (i) determine the cause of the gamma-ray log response, which typically shows a sequence of interbedded sands and shales; (ii) determine the nature and characteristics of the samples contributing to oil production and (iii) determine possible environments of deposition. Approximately 20 thin sections were made, half of which were carbon-coated for SEM analysis. 10 specimens were subsampled from core material also for SEM analysis.

RESULTS

Log Response

The gamma ray log response of the Lower Amaranth Formation indicates a shaly sand lithology. In reality the lithology is a complex mixture of reddish-brown interbedded siltstones, sandstones and shales. The gamma ray log measures the natural radioactivity in formations. Generally as the shale content increases, the gamma ray log response increases because of the concentration of radioactive material in shale. However, clean sandstones (i.e low shale content) may also produce a high gamma ray response if the sandstone contains potassium feldspars, micas and glauconite. The lower gamma ray readings in wells 6-11 and 4-14 are due to cleaner (i.e. less potassium feldspar, micas and glauconite) beds within the Lower Amaranth Formation.

Porosity Development

The overall average porosity is about 15%. This porosity varies from primary intergranular to secondary microintercrystalline in the recrystallized dolomitic matrix. The selective removal of feldspar grains by dissolution also contributes secondary porosity. Most of the primary intergranular porosity has been destroyed by anhydrite cementation. Pore shapes vary from irregular openings in matrix material and anhydrite nodules to rounded and elongated openings due to feldspar dissolution. Porosity development and preservation are controlled by anhydritization and dolomitization. The best developed porosity is in well 4-14-1-24 W1 due to the dissolution of grains and dolomitization. 4-14 has also produced the highest amount of oil to date (compared to the well at 6-11-1-24 W1).

Diagenesis

Diagenesis in the Lower Amaranth Formation includes compaction of grains, dolomitization, hematization, anhydritization and the dissolution of feldspars.

Depositional Environment

The Lower Amaranth Formation has typically been associated with tidal flat sedimentation. Based on the restrictions of this study to the petrographic analysis of two wells the environment of deposition was difficult to determine but was probably an intermittent, shallow, possibly restricted environment associated with marine conditions.

PETROGRAPHY

The sediments are composed of clasts and matrix material. Clasts are dominantly fine to medium sand size quartz, feldspar, and anhydrite. The fine to very fine sand to silt size matrix consists of dominantly quartz & feldspar that is cemented by anhydrite, clay minerals (i.e muscovite, chlorite) and hematite.

Anhydrite

Anhydrite is present mainly as distorted, subrounded nodules and mosaic cement. The cement preferentially fills primary porosity and is preferentially associated with the coarser-grained quartz. Anhydrite is also partially replaced by dolomite.

Quartz:

Quartz clasts make up 65% (on average) of the mineral components. Subangular to subrounded quartz is present in the very fine-grained matrix and as fine- to medium-grained rounded to well-rounded lenses or pods. Quartz lenses are commonly cemented with anhydrite. Also occurs as inclusions in anhydrite nodules.

Potassium Feldspar:

Feldspars are generally well preserved although some corrosion/dissolution occurred. noted. Feldspars are typically present as unaltered grains, partially altered grains and completely dissolved grains (identified on the basis of remanent feldspar in pore spaces). The dissolution of feldspars contributes secondary porosity. Subangular to subrounded grains are present as fine-

to medium-grained clasts and in the very fine-grained matrix. Also occurs as inclusions in anhydrite nodules.

Hematite:

Generally occurs as trace amounts (<1%) in the matrix, however it is significantly less abundant in the coarser-grained sand lenses. Fine-grained hematite, as well as clays and opaque grains, are scattered throughout the matrix or concentrated in patches &/or along preserved laminae. The presence of hematite causes the reddish-brown coloration of the cores.

Glauconite

Observed only in thin section with a microscope. Glauconite makes up less then 1% of the mineral constituents in Amaranth cores. It is, however, a good indicator of a marine influenced depositional environment.

Muscovite:

Muscovite occurs as fine- to very fine-grained laths in the matrix which often wrap around other grains, such as quartz and feldspar, due to compaction and subsequent distortion.

Chlorite:

Chlorite occurs as fine- to very fine-grained sheets in the matrix and pore throats, and is less than 3% in abundance.

Dolomite (calcite):

Dolomite occurs as a fine- to very fine- grained interlocking mesh of crystals as matrix/cement material. It is present as dolomite infilling pore spaces to dolomitization of the fine-grained sediments. Microintercrystalline porosity is present between dolomite grains. Also replaces anhydrite.

4-14-1-24 W1

EDAX: Ca, Mg
dolomite on qtz. gr.

depth: 910.0 m

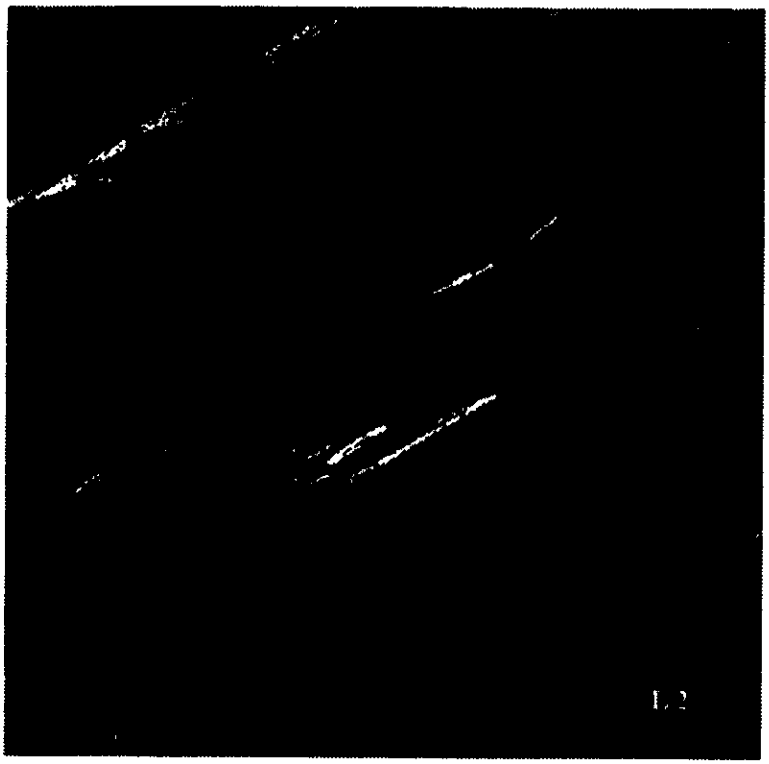

6-11-1-24 W1

feldspar

depth: 923 m

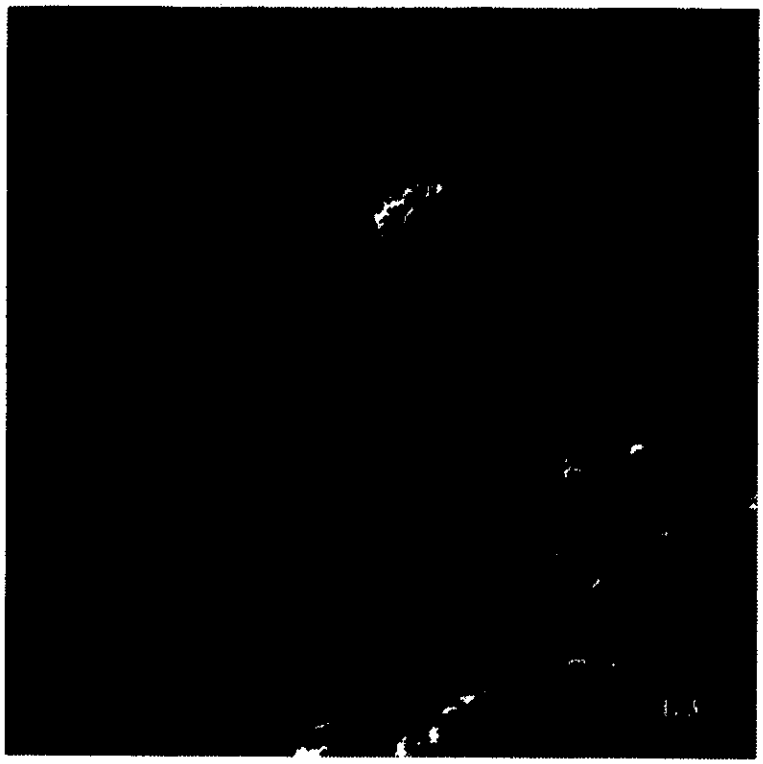

6-11

mostly anydrite
some feldspar

depth: 923 m

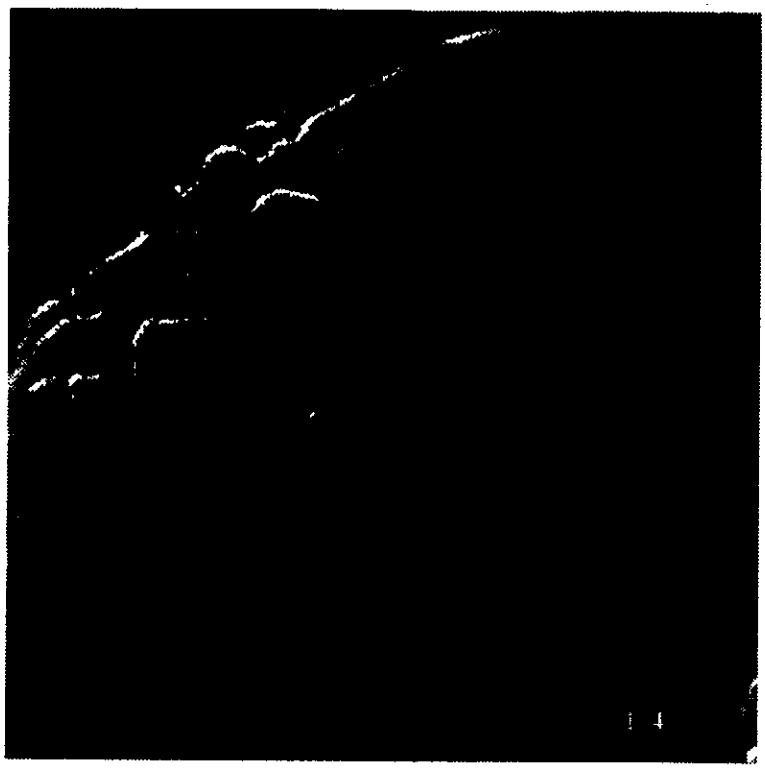

6-11

quartz?

depth: 923 m

4-14

dolomite xls
on qtz

depth: 922 m

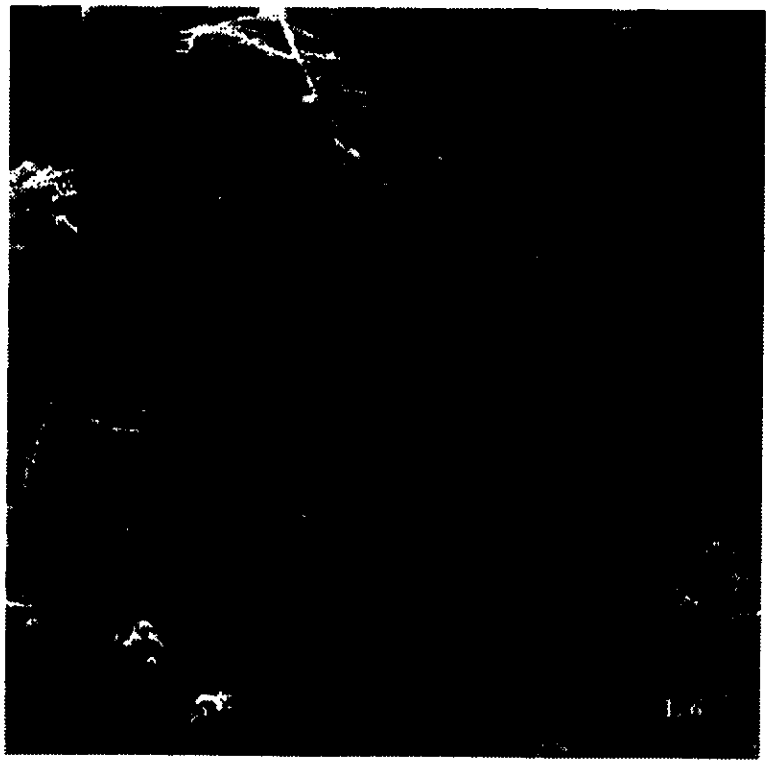

4-14

qtz x+l wrapped
in plant fibres

couldn't get
reading on xls
attached to fibres

depth: 922 m

20 um 1,09 KX

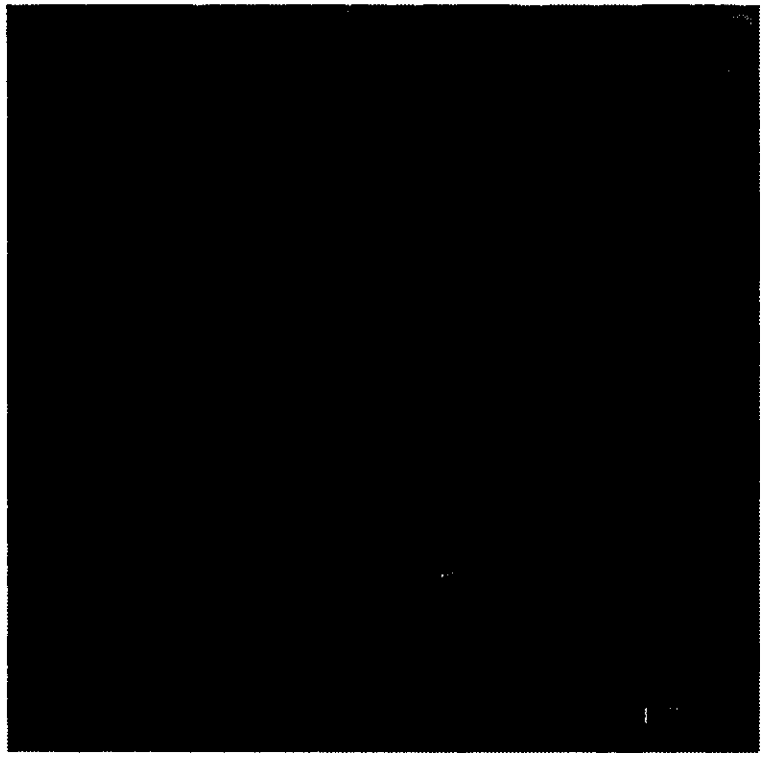

4-14

large anhydrite xl surrounded by quartz

depth: 922 m

4-14

anhydrite

depth: 922 m

4-14

anhydrite xl
with dolomite xls
in cleavage

depth: 922 m

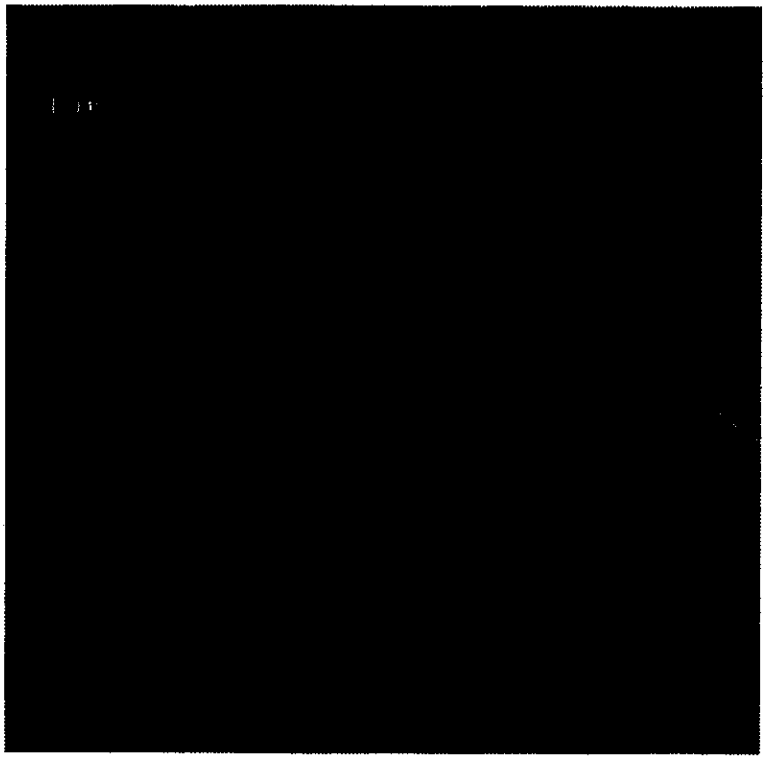

pore

4-14

dolomite xls
surrounding a
pore

depth: 922 m

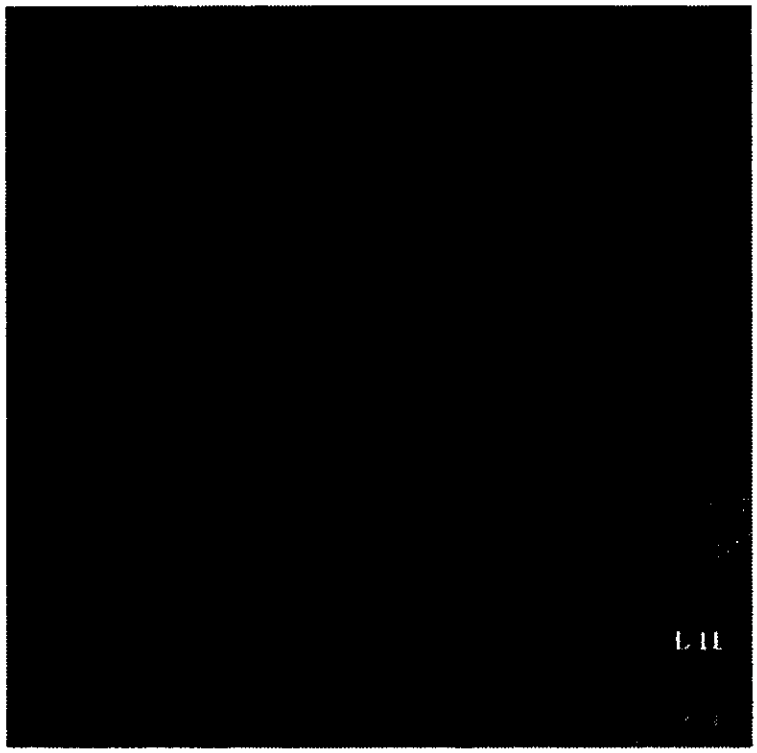

4-14

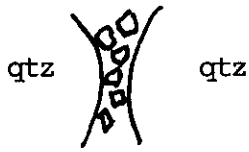

dolomite

depth: 922 m

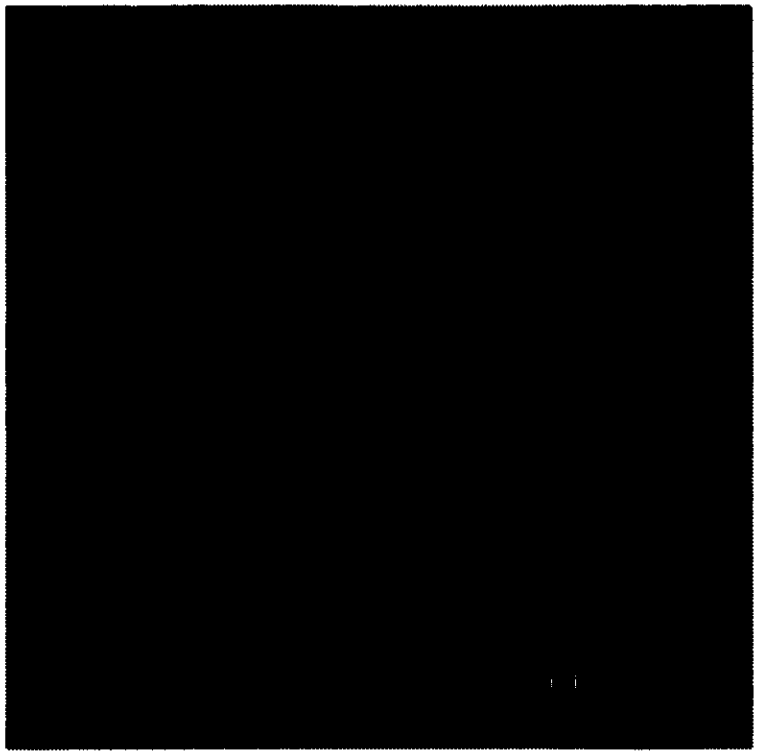

4-14

chlorite
EDAX i Ca, Fe,
K, Al, Si

depth: 923 m

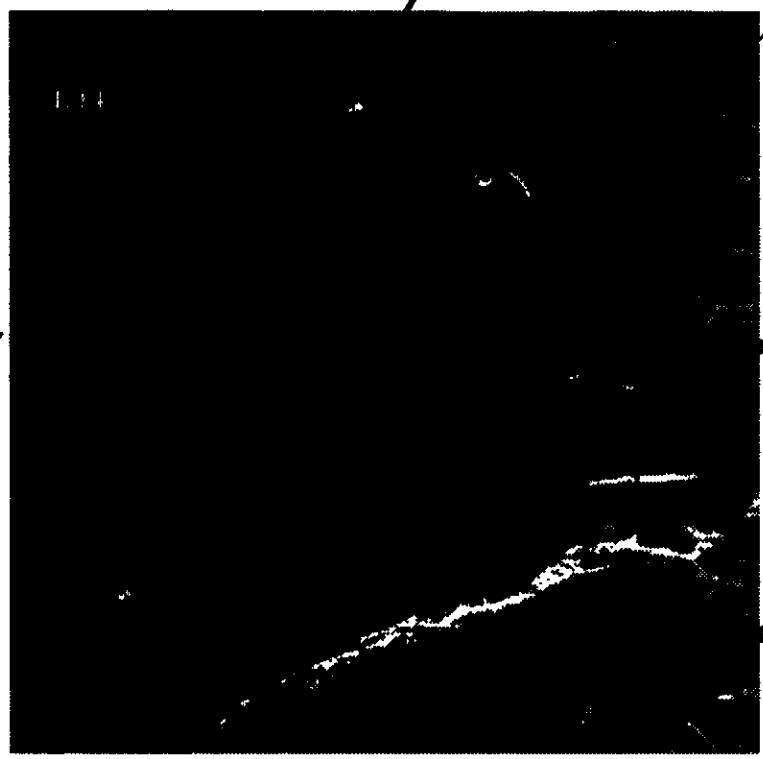

20 um

6-11

anhydrite surround and partially encrusted with cc/dolomite xls

depth: 918 m

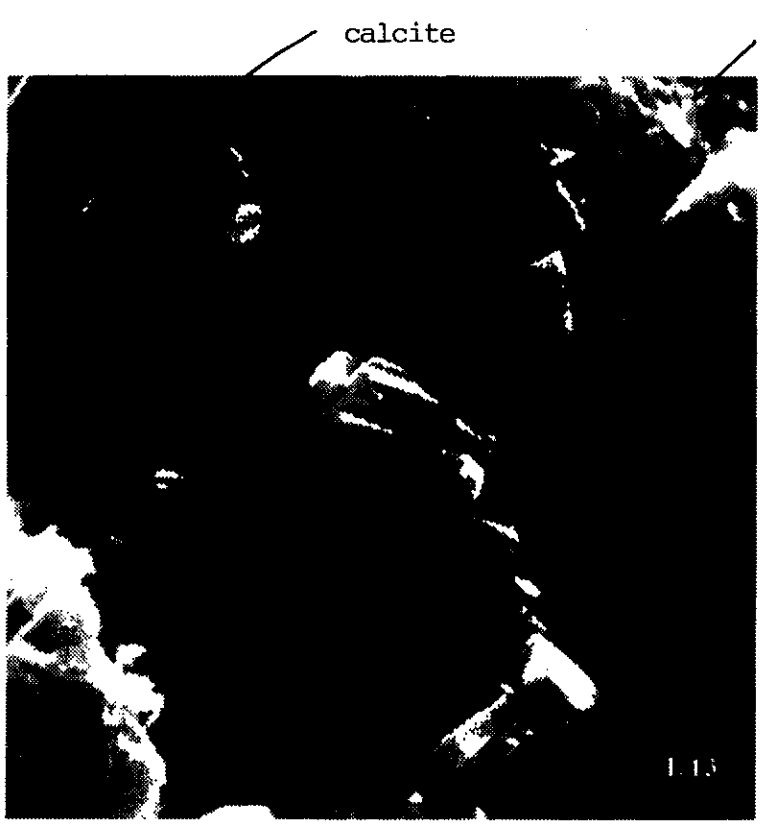

10 um

6-11

cc encrusting a quartz xl

depth: 918 m

6-11

feldspar encrusted by dolomite xls

note 'blind' leached ø

dolomite

depth 918 m

4-14

chlorite?

EDAX; Si, Fe, K, Al

- occupies pore spaces and encrusts grain

- fairly rare

- Elemental Iron present in some samples

Not pyrite
Not chorite

depth 918 m

50 um 634 x

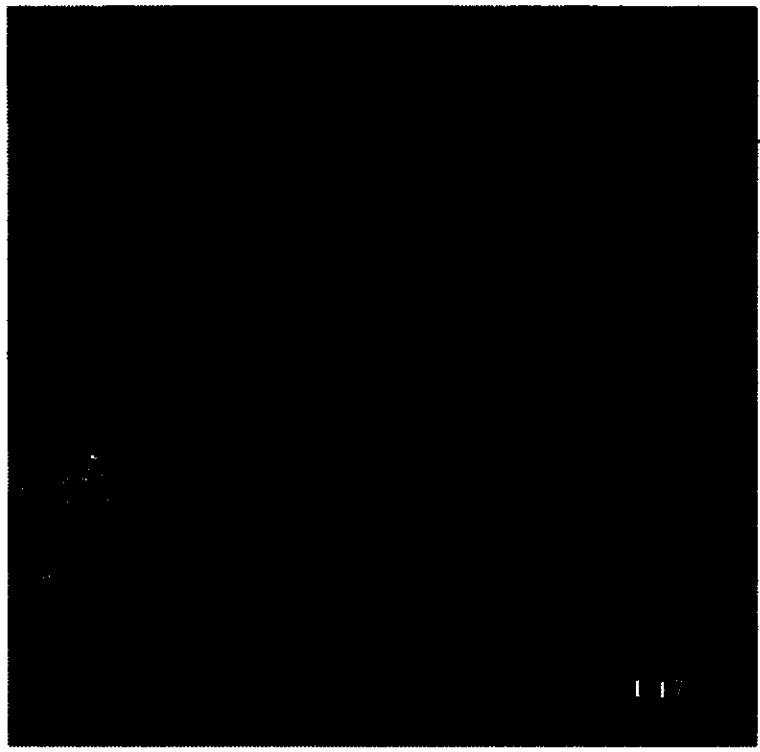

4-14

chlorite

depth 922 m

20 um 2,35 kx

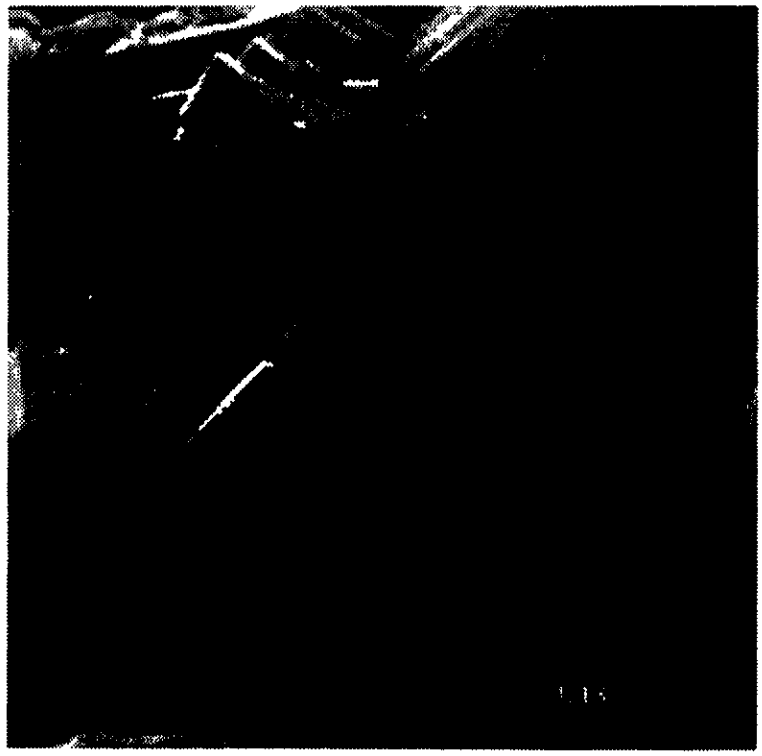

4-14

dolomite

depth 922 m

10 um 4,44 kx

Thin Sections

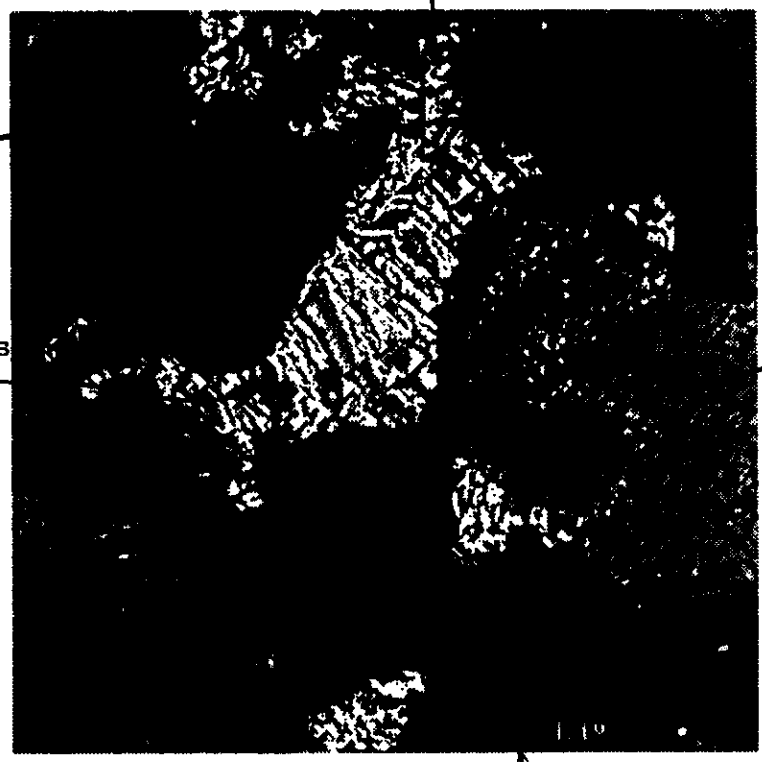

4-14

depth 922 m

100 um 397x

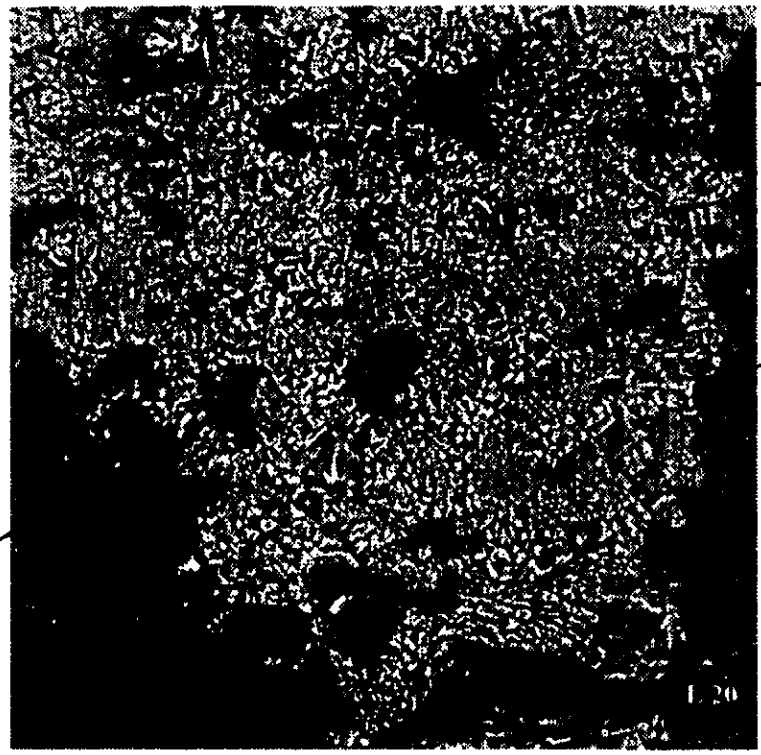

4-14

dolomite patches in anhydrite (as well as qtz)

- anhydrite nodule with some dolomite replacement of the anhydrite

depth 922 m

20 um 304 kx

200 um 197 kx

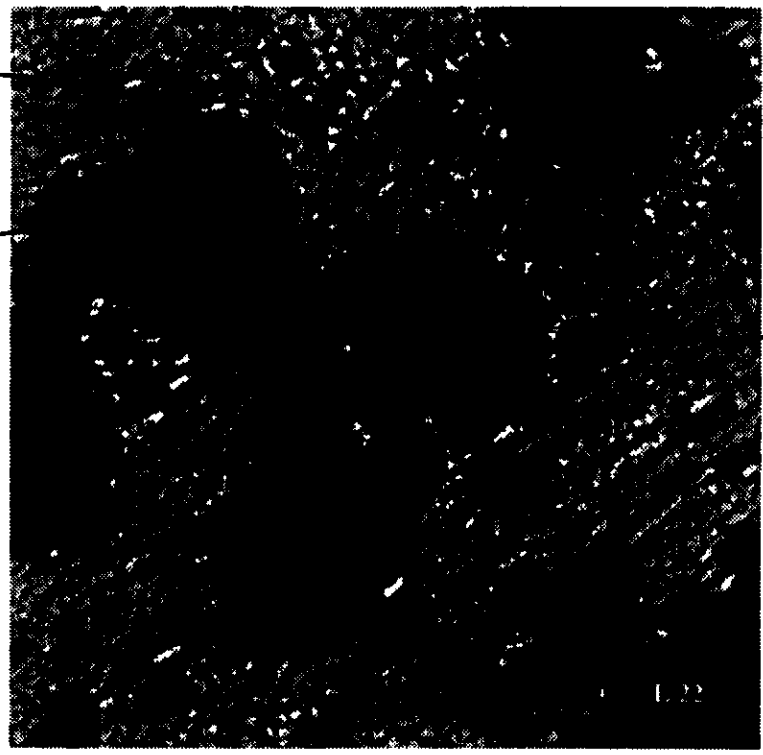

50 um 692 kx

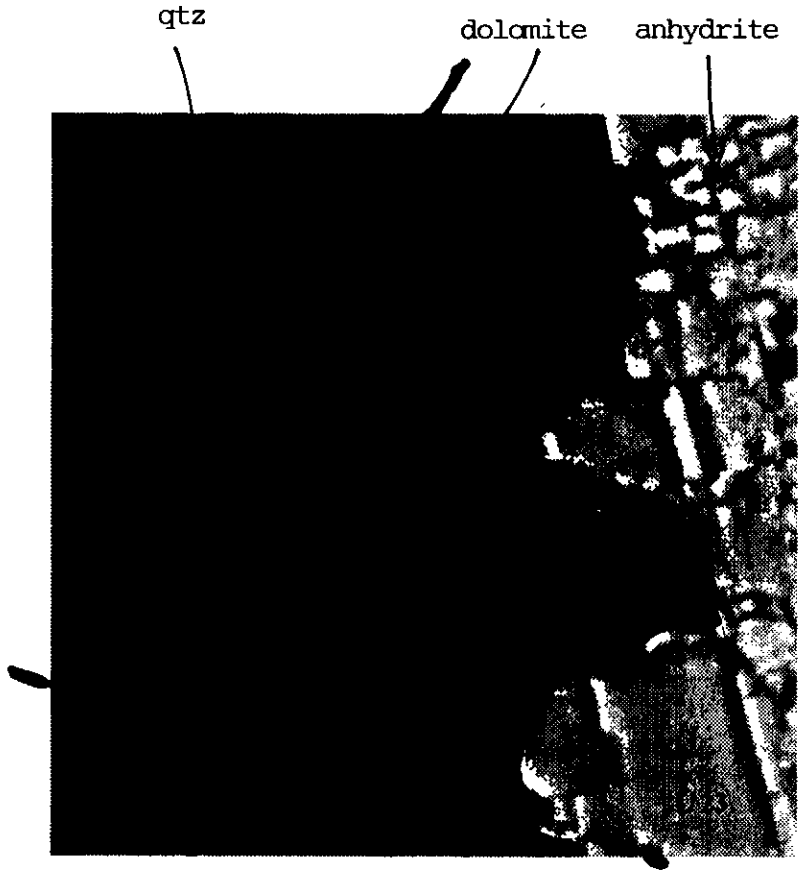

4-14

dolomite rim
anhydrite and quartz
grain followed by
anhydrite infill of
porosity

depth 922 m

20 um 1,23 kx

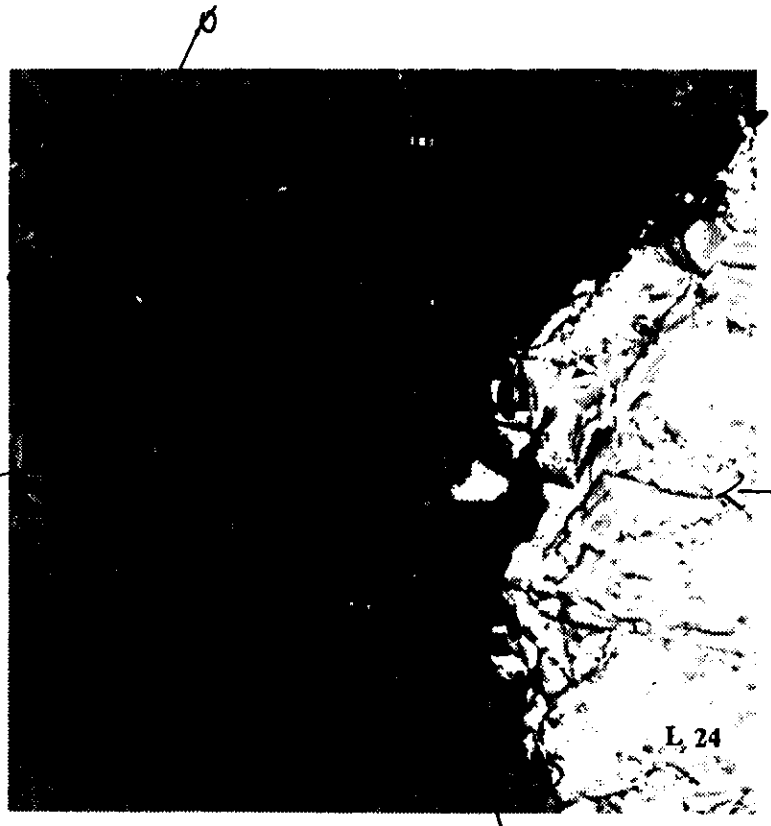

4-14

depth 922 m

50 um 615 x

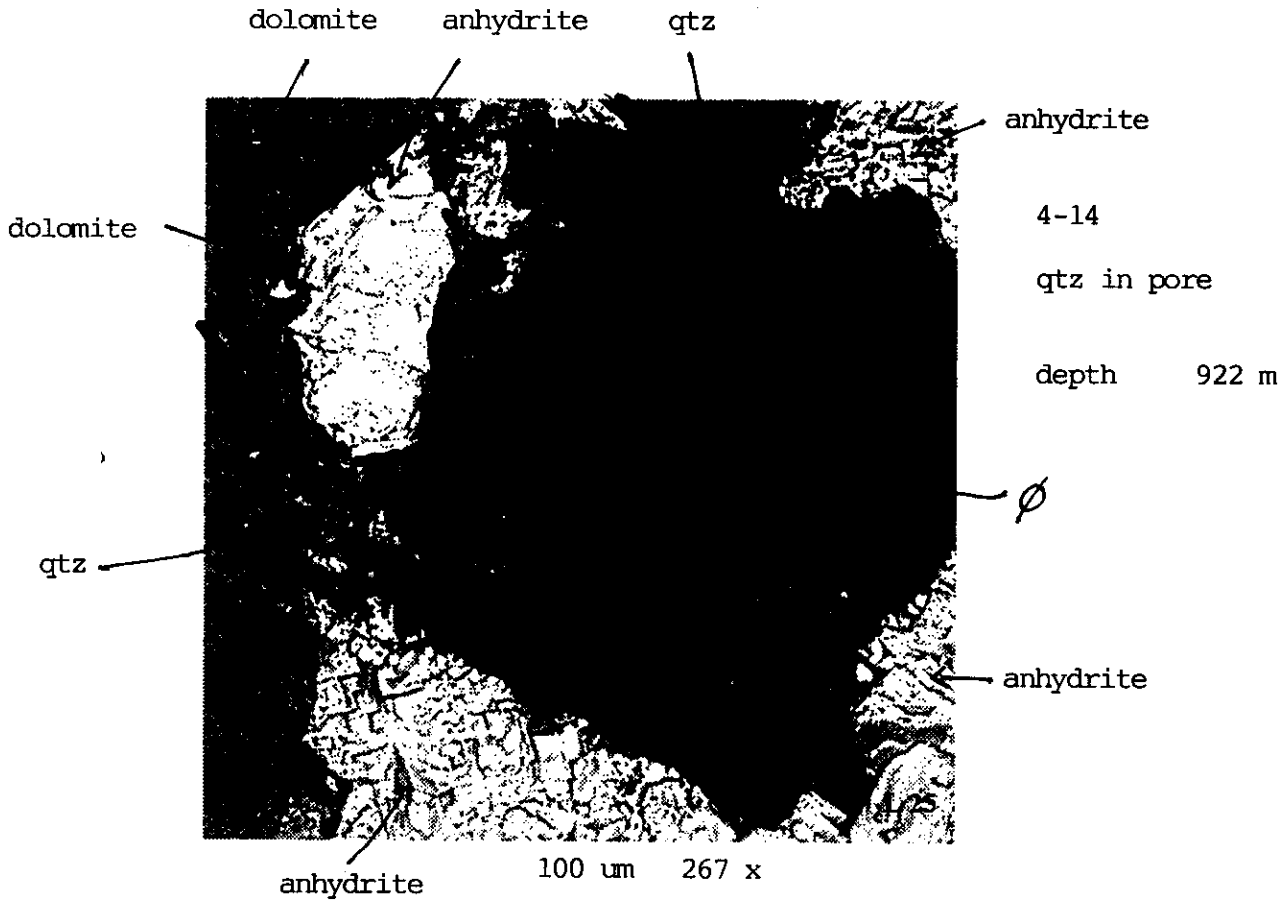
dolomite
anhydrite
qtz
anhydrite
dolomite
4-14
qtz in pore
depth 922 m
Ø
qtz
anhydrite
anhydrite
100 um 267 x

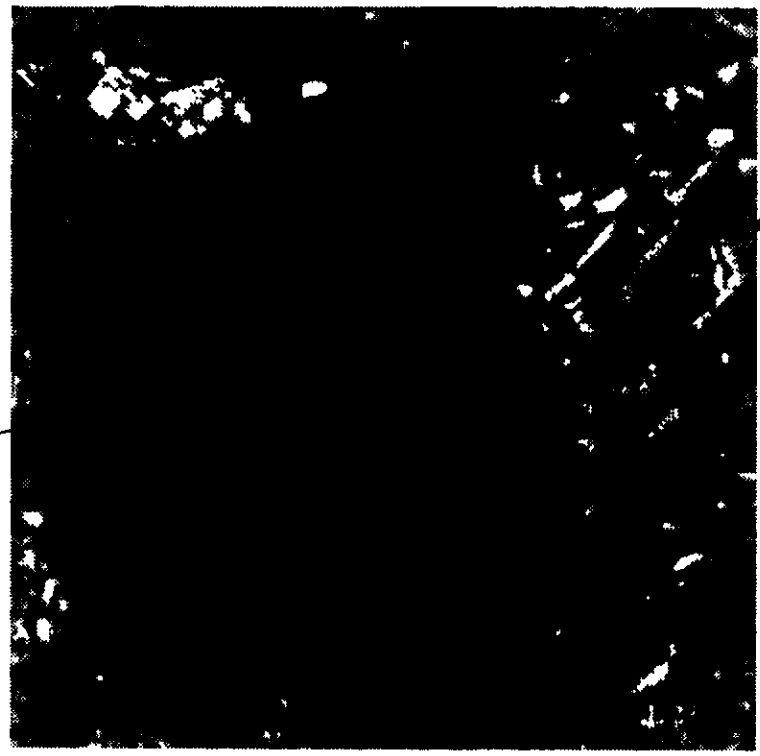

6-11

feldspar

matrix

qtz

50 um 905 x

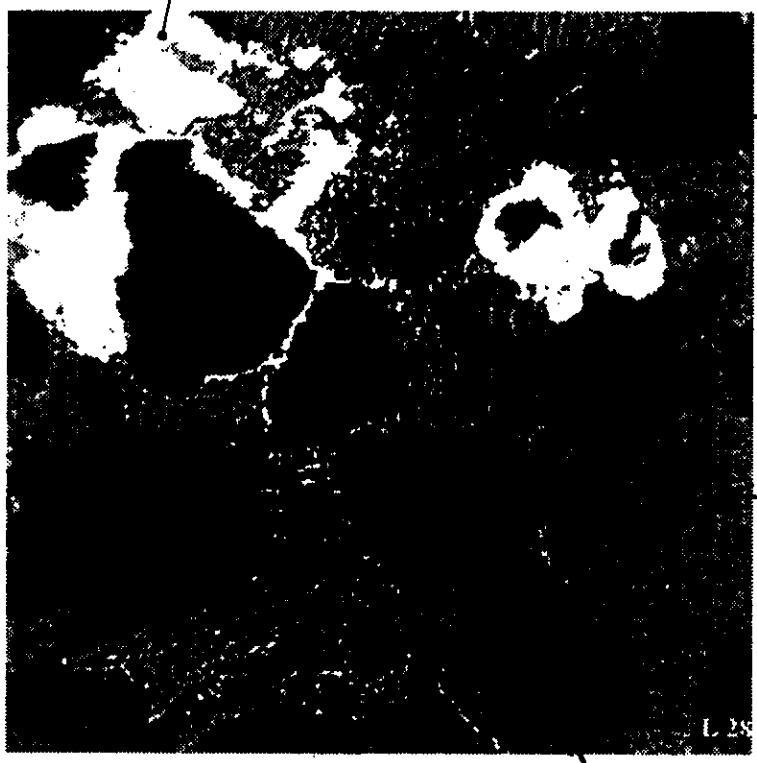

Fe

6-11

qtz

- iron rich zone have very low

anhydrite

depth 923 m

100 um 331 x

feldspar

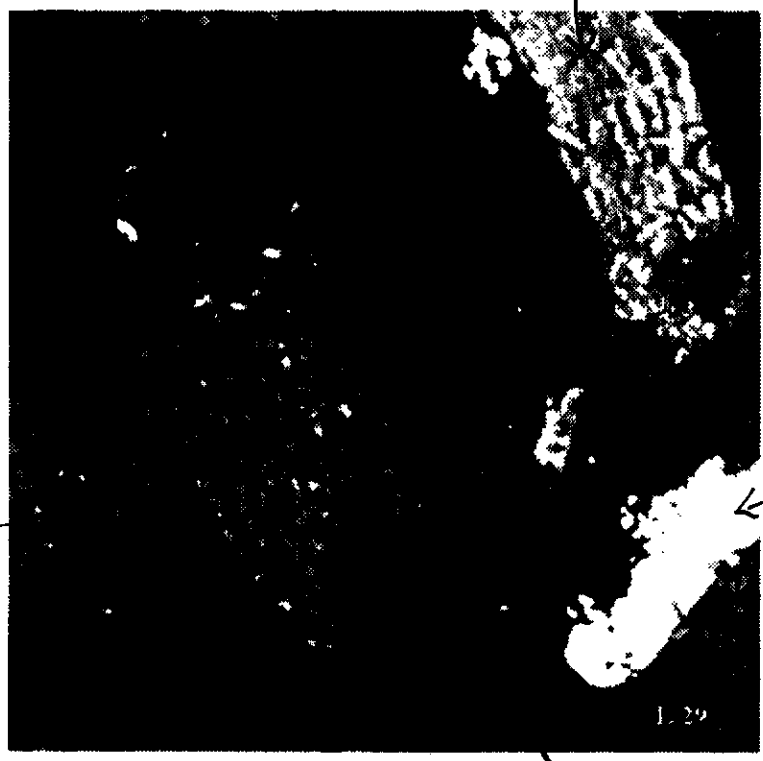
muscovite
6-11
matrix
length of feldspar
25 um
Fe
depth 923 m
pore
50 um 649 x

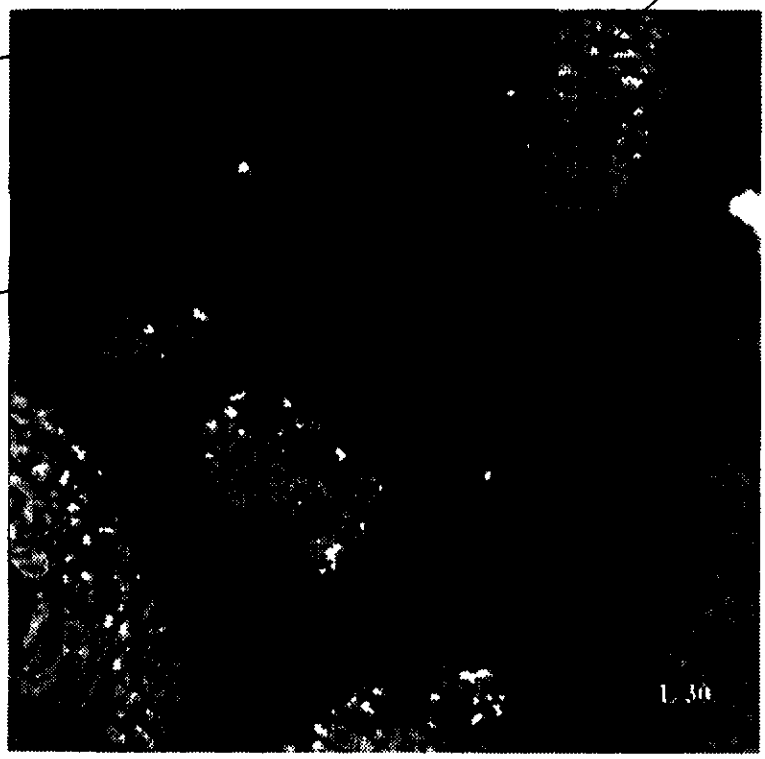
anhydrite
4-14
qtz
length of feldspar
25 um
depth 914 m
50 um 649 x

qtz length
is 100 um

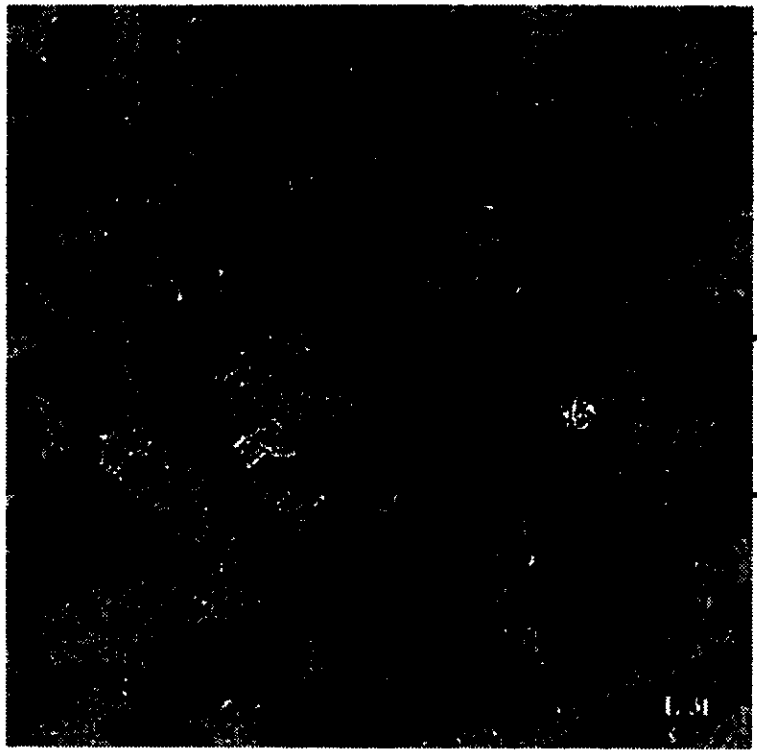

anhydrite

4-14

qtz

Ø

depth 914 m

200 um 164 x

Ø

6-11

qtz

anhydrite

feldspar

depth 926 m

100 um 376 x

6-11

? dissolution ϕ

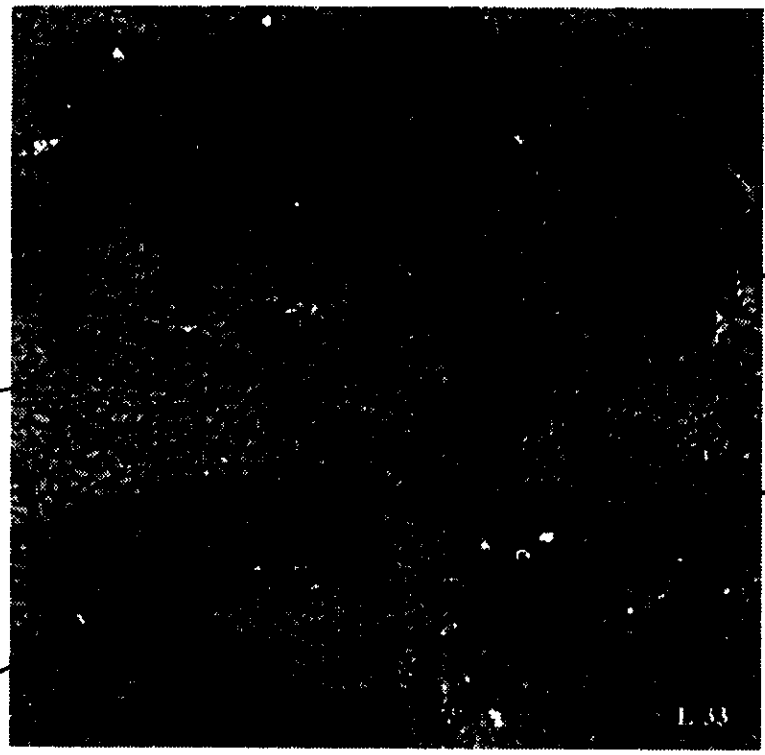

ϕ

feldspar
(100 um in
length)

qtz

ϕ

depth 926 m

100 um 370 x

dolomite

4-14

anhydrite

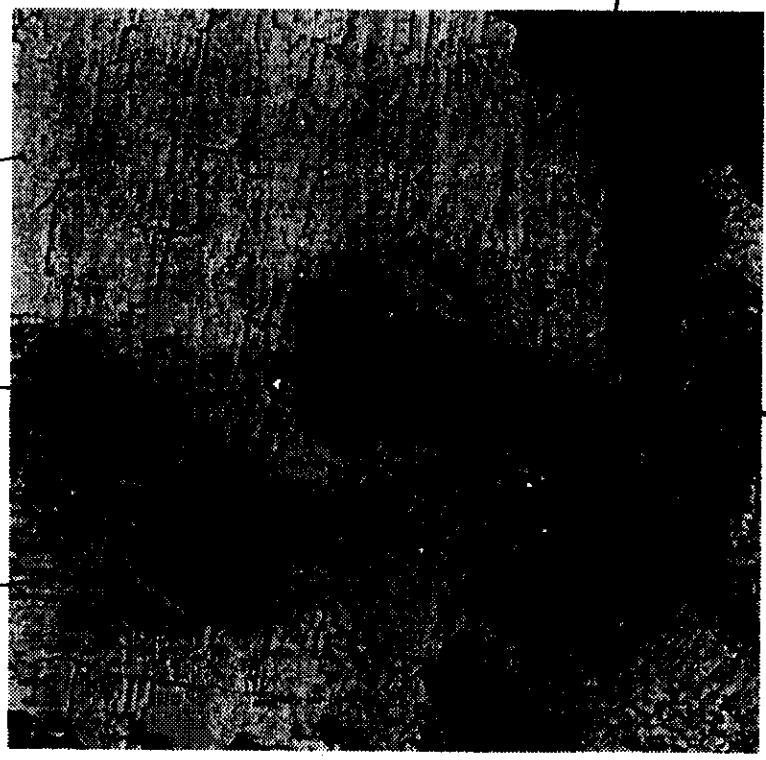

2 xls length
is 100 um dolomite

dolomite

qtz

depth 914 m

100 um 333 x

4-14

blow up of 36

feldspar dissolution

dolomite

depth 914 m

feldspar

blow up of below

- strongly resembles leiched fossil fragment

4-14

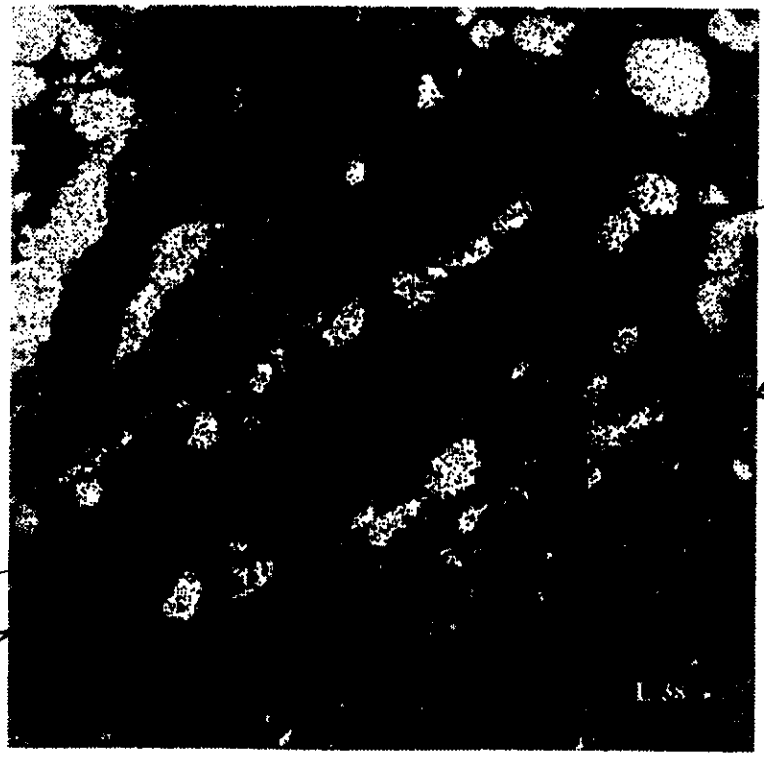

dolomite 'nodule' in qtz matrix

qtz (and other matrix material)

matrix material typically qtz, feldspar, ms (clays), hematite, anhydrite and other oxides

depth 914 m

length is ½ mm

dolomite

1 mm 29.7 x

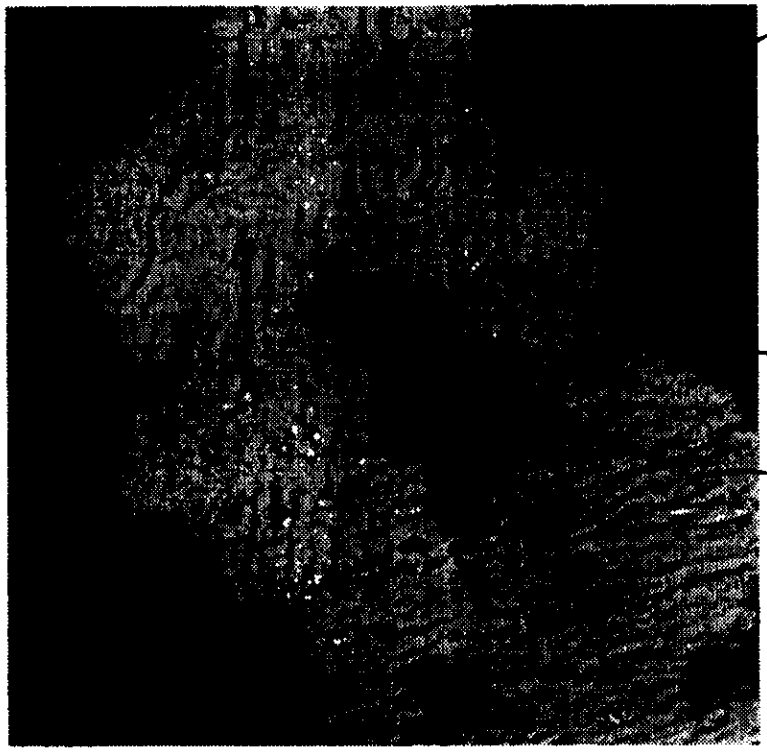

qtz

4-14

dolomite in anhydrite

dolomite

anhydrite

depth 914 m

50 um 535 x

Overall view of
a dolomite nodule
within a quartz matrix.
Nodule is porous

('L 38)

length is 200 um

4-14

all dolomite

feldspar

anhydrite

depth 914 m

200 um 133 x

4-14

depth 914 m

100 um 274 x